Treating muscle and brain alike: benefits of GSK3 inhibition in *mdx* mice

Bianca M. Marcella[a1,2], Emily N. Copeland[a1,2,3], Sophie I. Hamstra[a1,2], Briana L. Hockey[1,2], Jessica L. Braun[1,2,3], Mia S. Geromella[1,2], Kennedy C. Whitley[1,2], Colton J.F. Watson[4], Lucas A. Maddalena[5], Bradley J. Baranowski[3,4], Ahmad Mohammad[3,4], Sebastian Silvera[1,2], Ryan W. Baranowski[1,2], Evelyn C. Ochoa[1,2,3], Luc J. Wasilewicz[1,2], Robert W.E. Crozier[4], Riley E.G. Cleverdon[1,2], Shawn M. Beaudette[1,2], Rene Vandenboom[1,2], Brian D. Roy[1,2], Jeffrey A. Stuart,[5] Adam J. MacNeil[3], Rebecca E.K. MacPherson[3,4*], Val A. Fajardo[1,2,4,6*]

[a] These authors contributed equally

[1] Department of Kinesiology, Brock University, St. Catharines, ON, Canada
[2] Centre for Bone and Muscle Health, Brock University, St. Catharines, ON, Canada
[3] Centre for Neurosciences, Brock University, St. Catharines, ON, Canada
[4] Department of Health Sciences, Brock University, St. Catharines, ON, Canada
[5] Department of Biological Sciences, Brock University, St. Catharines, ON, Canada
[6] Lead contact

*Corresponding authors:

Val A. Fajardo, PhD
Associate Professor
Canada Research Chair (Tier II)
Department of Kinesiology
Brock University
St. Catharines, ON
L2S 3A1
vfajardo@brocku.ca

Rebecca E.K. MacPherson, PhD
Associate Professor
Department of Health Sciences
Brock University
St. Catharines, ON
L2S 3A1
rmacpherson@brocku.ca

Summary

In addition to progressive muscle wasting and weakness, many patients living with Duchenne muscular dystrophy (DMD) experience cognitive decline, which further compromises their quality of life. Here, we investigated whether inhibiting glycogen synthase kinase 3 (GSK3) in the DBA/2J *mdx* mouse model of DMD could benefit both muscle and brain health. Short-term treatment with the GSK3 inhibitor, tideglusib, reduced skeletal and cardiac muscle necrosis, leading to improvements in muscle contractility. Similar benefits were found when GSK3 inhibition via lithium supplementation was combined with voluntary wheel running. In the brain, GSK3 was found to be overactive in the hippocampus from *mdx* mice, and inhibiting GSK3 improved cognitive function. Further, this result was accompanied with reduced beta-secretase activity and increased clearance of β-amyloid. Altogether, our findings reveal GSK3 inhibition as a potential therapy for DMD – one aimed at enhancing muscle and brain health and overall quality of life.

Highlights (up to 4 points at 85 characters each including spaces)

- Tideglusib treatment attenuated muscle pathology and improved whole-body metabolism
- Voluntary wheel running and lithium supplementation improved muscle function
- GSK3 inhibition in the brain improved recognition memory in young and aged *mdx* mice
- GSK3 inhibition may enhance the quality of life of those living with DMD

Introduction

Duchenne muscular dystrophy (DMD) is a severe X-linked muscle wasting disorder that affects 1 in 5,000 males worldwide[1]. It is caused by the absence of functional dystrophin – a structural protein that provides membrane stability to muscle throughout strenuous contraction-relaxation cycles. Muscle integrity is compromised without dystrophin, leading to progressive muscle wasting and weakness, and as a result, patients with DMD are often wheelchair-bound by their teenage years[2]. There is no cure for DMD, and despite recent advances in disease management, the average lifespan for an individual with DMD ranges from 20-30 years as they unfortunately succumb to cardiorespiratory failure[3].

In addition to muscle wasting and weakness, a substantial proportion of boys living with DMD (30-40%) present with cognitive impairments and neurobehavioral changes such as low intelligence quotient (IQ) scores (<70)[4] and reading and learning deficits[5]. Combined, impaired muscle and cognitive function can drastically lower one's quality of life. Treatments aimed at improving both muscle and brain pathology could therefore have immeasurable benefits on the lives of those suffering from DMD. Exploring the cellular mechanisms that underpin dystrophic pathology in both muscle and brain is important as it may reveal novel and universal therapeutic targets and intervention strategies.

Glycogen synthase kinase 3 (GSK3) is a serine/threonine (Ser/Thr) kinase that was first identified for its role in regulating glycogen synthase in muscle but is now known to phosphorylate more than 100 substrates throughout the body[6]. There are two GSK3 isoforms, GSK3α and GSK3β, with the latter being the most expressed and active isoform found within muscle[7] and brain[8]. GSK3 can be inhibited via Ser phosphorylation (Ser21 on GSK3α and Ser9 on GSK3β), which prevents GSK3 from binding with its downstream targets[6]. In muscle, the

inhibition of GSK3 promotes greater muscle mass via an increase in protein synthesis and myoblast fusion, and a decrease in proteolytic degradation (for review see ref[9]). Furthermore, we and others have shown that the inhibition of GSK3 in skeletal muscle can increase the proportion of type I and IIA oxidative muscle fibers by activating the transcription factor, nuclear factor of activated T cells (NFAT)[10,11]. DMD primarily affects the type II glycolytic fibers[12,13]; therefore, promoting the oxidative phenotype via GSK3 inhibition could attenuate dystrophic pathology[12,14-16].

In the brain, the inhibition of GSK3 has been viewed as a viable therapeutic strategy for many neurodegenerative diseases such as Parkinson's and Alzheimer's disease (AD)[17]. Recently, we identified an AD-like pathology in young (10-12 week old) DBA/2J (D2) *mdx* mice, where these mice displayed recognition memory deficits and a shift in brain biochemistry that favoured the production of β-amyloid (Aβ) peptides[18]. GSK3 is a has a well-established pathological role in AD where its overactivation can increase the content and activity of beta-secretase 1 (BACE1), which catalyzes the rate-limiting step in amyloidogenesis[19]. Thus, GSK3 inhibition in *mdx* mice may improve cognitive function by mitigating AD-like pathology – all while improving muscle health.

To test whether GSK3 inhibition can enhance muscle and brain health for DMD, we investigated the effects of inhibiting GSK3 in the DBA/2J (D2) *mdx* mouse model. We first examined the effects of short-term treatment with tideglusib. This drug belongs to the thiadiazolidindione family and is a non-ATP competitive GSK3 inhibitor that is currently in clinical trials for supranuclear palsy, AD, and myotonic dystrophy type 1 (DM1)[20,21]. Next, we investigated the combined effects of voluntary wheel running (VWR) and GSK3 inhibition via lithium (Li) supplementation, a natural GSK3 inhibitor. VWR improves both muscle and brain

health in various mouse models[22-24]; however, its effect, if any, on cognitive function in D2 *mdx* mice remains unknown. Furthermore, it is unknown if the benefits of VWR in *mdx* mice can be amplified with GSK3 inhibition. This would be clinically relevant as only mild to moderate intensity exercise programs are suggested for those living with DMD[25,26], which highlights a need for adjuvant therapies.

RESULTS

Tideglusib treatment reduces muscle necrosis and improves muscle contractility

We first determined whether GSK3β content and activation status, as indicated by the levels of inhibitory Ser9 phosphorylation, would be different in muscles obtained from D2 *mdx* mice compared with WT. At 10-12 weeks of age, and across the extensor digitorum longus (EDL), diaphragm, and heart, we did not observe any differences in total or phosphorylated GSK3β levels (Figure 1A-C). Since GSK3 is a constitutively active enzyme[27], we next assessed the effects of inhibiting GSK3 in D2 *mdx* mice by using tideglusib. Mechanistically, tideglusib irreversibly binds to GSK3 and holds it in an inactive state[28]. While this is its primary mode of inhibition, tideglusib and other thiadiazolidinone compounds can also reduce total GSK3 content and increase inhibitory Ser9 phosphorylation[29,30]. In support of this mechanism, we found that 2 weeks of tideglusib treatment reduced GSK3β content across skeletal and cardiac muscle when compared with vehicle controls (Figure 1D-E). We also found greater Ser9 phosphorylation in these muscles after tideglusib treatment (Figure 1D and F).

After assessing EDL muscle histopathology, we found that tideglusib treatment significantly reduced muscle necrosis and serum creatine kinase (CK) levels (Figure 1G-I). Tideglusib treatment also lowered muscle nitrocysteine and nitrotyrosine content, indicating

lesser oxidative stress (Figure S1). Tideglusib treatment led to a significant improvement in EDL specific force generation (Figure 1J) and increased the cross-sectional area (CSA) of all fibre types in the EDL (Figure 1K-L) – a result consistent with the known hypertrophic effect of GSK3 inhibition[9,31]. Moreover, and in agreement with the repressive action of GSK3 on the oxidative fibre type[9,10], tideglusib treatment significantly lowered the proportion of glycolytic fibres (IIB and IIX) while increasing the proportion of oxidative (I and IIA fibres) (Figure 1M). Further, plantaris muscles from tideglusib treated *mdx* mice had greater utrophin expression when compared with vehicle treated mice (Figure 1N). Utrophin is a dystrophin homolog that can provide compensatory membrane stability[32,33], and its expression is controlled by NFAT signalling and is thus tightly tied to the oxidative myogenic program[12,13,34].

Collectively, these data show that tideglusib treatment in 10-12 week-old D2 *mdx* mice improved EDL muscle size, overall muscle quality and strength. These benefits of tideglusib treatment also extend to aged (28-30 week-old) D2 *mdx* mice with tideglusib lowering serum CK levels and improving specific force production (Figure S2). This is important given that dystrophic pathology in D2 *mdx* mice progressively worsens with age[35-37].

Tideglusib treatment improves diastolic function in young D2 mdx mice

Table 1 shows that in 10-12 week old mice there were no differences in measured left ventricle (LV) mass relative to body mass across the three experimental groups. However, signs of concentric remodelling with lower left ventricle internal diameter (LVID) and higher relative wall thickness (RWT) were found in both *mdx* groups compared with WT. Furthermore, end-systolic volume (ESV) was lower in vehicle treated and tideglusib treated D2 *mdx* mice compared with WT. There were no differences in stroke volume (SV), heart rate, or cardiac

output across groups, but % ejection fraction (%EF) and fractional shortening (%FS) were higher in both *mdx* groups compared with WT.

We also performed pulsed wave (PW) doppler analysis of the mitral valve inflow. Table 1 shows no differences in E wave velocity amongst the groups; however, A wave velocity was slower in tideglusib treated *mdx* mice when compared with WT mice. In turn, the tideglusib treated *mdx* mice had the highest E/A ratio, being significantly different from WT mice. Further, E wave deceleration time (DT) was significantly shorter in the vehicle treated *mdx* mice compared with both WT and tideglusib treated *mdx* mice, which is suggestive of increased LV stiffness[38]. Finally, when examining isovolumic contraction and relaxation time (IVCT and IVRT, respectively), we found that IVRT was prolonged in the vehicle treated *mdx* mice compared with both WT and tideglusib treated *mdx* mice. There were no differences in IVCT. Overall, these results indicate that young (10-12 week old) *mdx* mice show signs of concentric remodelling; and while systolic function is intact, and apparently even enhanced, diastolic dysfunction and reduced compliance is observed in vehicle treated D2 *mdx* mice, but not in tideglusib treated D2 *mdx* mice. This apparent restoration of diastolic function and cardiac compliance with tideglusib treatment is likely due to a reduction in muscle oxidative stress (Figure S1), as we did not observe any differences in sarco(endo)plasmic reticulum Ca^{2+}-ATPase (SERCA) function or muscle fibrosis (Figure S3 and S4).

Tideglusib treatment reverses various metabolic abnormalities found in D2 mdx mice

Previous studies have shown that *mdx* mice backcrossed onto a DBA/2J or C57BL/10 background present with a higher daily energy expenditure compared with WT mice[39,40]. As this hypermetabolic phenotype is largely due to the energetic costs associated with constant muscle

degeneration/regeneration cycling, we next examined the effects of tideglusib treatment on daily energy expenditure. In both young (10-12 weeks) and aged (28-30 weeks) D2 *mdx* mice, tideglusib treated groups had lower energy expenditure when compared with vehicle treated groups (Figure 2A and B). This effect was not due to any changes in daily cage ambulation (Figure 2C and D). Furthermore, the hypermetabolic phenotype in *mdx* mice has been previously shown to lower body fat content in C57BL/10 *mdx* mice, resulting in less whole-body lipid supply, which raises the respiratory exchange ratio (RER)[40]. In our hands, D2 *mdx* mice also have a higher RER when compared with WT mice (Figure S5). Corresponding well with the reduction in energy expenditure, both young and aged tideglusib treated D2 *mdx* mice have higher body fat content when compared with vehicle treated mice, though this effect was most prominent at 28-30 weeks of age (Figure 2E and F). Moreover, tideglusib treated mice had lower RER values when compared with vehicle treated mice (Figure 2G and H).

We next examined the effects of GSK3 inhibition via tideglusib treatment on insulin sensitivity since *mdx* mice are already known to be insulin resistant[41]. Insulin tolerance tests showed that tideglusib treatment improved insulin sensitivity with a reduction in the area-under-the-curve (AUC) and a greater percent decline in blood glucose when compared to vehicle treated *mdx* mice (Figure 2I-L). In contrast, the *mdx*-vehicle group showed very little response to insulin and many of the mice displayed a slight increase in blood glucose levels (Figure 2I and L). Collectively, these results suggest that the improvement in overall muscle health and integrity observed with tideglusib treatment reversed several metabolic alterations commonly found in *mdx* mice.

Lithium and voluntary wheel running improves muscle function and metabolism in mdx mice

We next investigated the combined effects of exercise and GSK3 inhibition on muscle form and function in young (10-12 week old) *mdx* mice. VWR was chosen as the mode of exercise given its low intensity and minimal stress added to the mouse[42]. To further minimize stress, we treated the mice with the GSK3 inhibitor, Li, as it could be provided easily through drinking water rather than performing oral daily gavage as with tideglusib. Li is a natural inhibitor of GSK3 and is most commonly used for the treatment of bipolar disorder[43]; however, its clinical use must occur within a narrow therapeutic range of 0.5-1.0 mM serum Li concentration to avoid potential adverse effects on various tissues[43]. Here, we treated *mdx* mice with a low dose of lithium chloride (50 mg/kg/day via drinking water) for 6 weeks, which resulted in a serum Li concentration of 0.15 ± 0.05 mM (n = 9). Similar to tideglusib, Li supplementation with VWR improved specific force production in *mdx* soleus and EDL muscles (Figure 3A-B). In the soleus, WT mice produced significantly more force than *mdx* sedentary (*mdx*-SED) and *mdx*-VWR groups, but no differences were found when comparing WT mice with *mdx*-VWRLi mice (Figure 3A). Furthermore, the soleus from the *mdx*-VWRLi group produced significantly more force when compared to the *mdx*-SED group at sub-maximal and maximal frequencies (Figure 3A). In the EDL, WT mice produced significantly more force compared with all *mdx* groups across submaximal and maximal frequencies (Figure 3B). This was particularly evident when WT was compared with the *mdx*-VWR group, whereby significant differences were detected at 20 and 40 Hz and could be suggestive of worsened muscle strength with VWR (Figure 3B). However, this was not found when *mdx*-VWR mice were supplemented with Li as the EDL from *mdx*-VWRLi mice produced significantly more force when compared with *mdx*-SED (160Hz) and *mdx*-VWR (20, 40, 80 and 160 Hz) groups (Figure 3B).

The improvements in contractile function observed in the *mdx*-VWRLi mice were associated with significantly lower markers of oxidative stress (total nitrotyrosine and nitrocysteine) compared with *mdx*-SED mice (Figure 3C-D). Histological analysis showed that the EDL muscles from *mdx* mice are more necrotic when compared with the soleus with a significant main effect of muscle type (Figure 3E-F). This was expected as glycolytic muscles are more susceptible to dystrophic pathology[12,13]. Additionally, a significant main effect of condition indicated that muscles from *mdx*-VWRLi mice have significantly lower levels of necrosis when compared with those from the *mdx*-SED group (Figure 3E-F). We also assessed utrophin expression, which was higher in quadriceps muscles from *mdx* mice subjected to VWR (Figure S6). Although Li supplementation did not provide any additive effect (Figure S6), this result is consistent with other VWR studies conducted in *mdx* mice[24].

High frequency ultrasound analysis showed that *mdx*-VWRLi mice had significantly prolonged DT when compared with *mdx*-SED and *mdx*-VWR mice (Table 2). These results are similar to those found in young tideglusib treated mice (Table 1). There were no differences between groups when assessing cardiac muscle morphology (i.e., internal diameter or relative wall thickness); however, *mdx*-VWR mice had significantly lowered %EF and %FS compared with *mdx*-SED mice, which is indicative of worsened cardiac contractile function in response to VWR. Importantly, these effects were not detected between *mdx*-SED and *mdx*-VWRLi mice (Table 2).

With respect to metabolic alterations, and similar to that observed with tideglusib (Figure 2), the *mdx*-VWRLi mice had the lowest RER compared with the *mdx*-SED mice, which is indicative of enhanced lipid oxidation (Figure S7). The *mdx*-VWRLi mice were also more insulin sensitive when compared with the other *mdx* groups (Figure 3G-I). Specifically, insulin

tolerance tests showed that *mdx*-SED mice were insulin resistant compared with WT, *mdx*-VWR, and *mdx*-VWRLi mice (Figure 3G). While VWR improved insulin tolerance in *mdx* mice, Li supplementation provided an additive effect, whereby *mdx*-VWRLi mice had the lowest AUC and largest percent decline in blood glucose levels compared with all *mdx* groups and without any differences in baseline glucose levels (Figure 3H-J). Furthermore, the metabolic and contractile benefits of Li were found with half the exercise volume compared with *mdx*-VWR mice. After measuring average daily distance travelled and total distance travelled, we found that the *mdx*-VWRLi group ran significantly less (-50%) than the *mdx*-VWR group when given access to a cagewheel (Figure 3J-K). Thus, these results show that despite running less, Li supplementation combined with VWR can significantly improve specific force production, reduce oxidative stress/necrosis, and enhance oxidative lipid metabolism and insulin sensitivity.

GSK3 inhibition with Li or tideglusib improves cognitive function in mdx mice

GSK3 is a well-known target for various neurodegenerative diseases, and unlike muscle, our results show that GSK3β content is elevated and less phosphorylated in the hippocampus from D2 *mdx* mice compared with WT mice (Figure 4A). This indicates that GSK3 is more active in the *mdx* brain. Using a novel object recognition test (NORT) to investigate spatial/recognition memory, we found that VWR did not improve total or novel object investigation time when compared with *mdx*-SED mice (p = 0.87 and p = 0.88, respectively Fig. 4B-C). In contrast, *mdx*-VWRLi mice had significantly greater total and novel object investigation time when compared with *mdx*-SED mice (Figure 4B-C). In fact, *mdx*-VWRLi mice also had greater novel investigation time compared with *mdx*-VWR mice (Figure 4C). These effects were not due to any differences in distance travelled in the testing arena (Figure

4D), which is an important parameter to consider given that *mdx*-VWRLi mice had shown improvements in muscle health and function (Figure 3). In our recent work, we found that D2 *mdx* mice exhibited AD-like pathology with an alteration in brain biochemistry favouring the production of pathological Aβ peptides[18]. BACE1 catalyzes the rate-limiting step in Aβ production and GSK3 overactivation increases BACE1 expression and activity in the brain[19]. While we did not find any differences in BACE1 content in our previous work[18], in the present study, we found that Li supplementation reduced BACE1 activity, with *mdx*-VWRLi mice having lower BACE1 activity compared with *mdx*-SED mice (Figure 4E).

In addition to the production of Aβ by BACE1, we also examined circulating Aβ as a proxy of vascular Aβ clearance. The pathological accumulation of Aβ oligomers in the brain can theoretically result from an overproduction and/or diminished clearance from the brain; and in sporadic AD, which constitutes >90% of individuals with AD[44,45], impaired Aβ clearance is known to be a key factor leading to Aβ accumulation[46]. Though the clearance of Aβ can occur through enzymatic degradation or non-enzymatically through transendothelial trafficking to circulating blood, the latter vascular pathway is the major route of removal from the brain[47]. Our results show that all *mdx* groups had greater levels of serum Aβ when compared with the healthy WT mice (Figure 4F). This result is consistent with the human pathology, as it was previously shown that patients living with DMD also present with greater levels of circulating Aβ peptides[48]. We believe that this could be a compensatory response aimed at clearing Aβ from the brain. Here, our results show that the *mdx*-VWRLi group had the highest levels of circulating Aβ, being significantly different from the *mdx*-SED group (Figure 4F), which is suggestive of greater Aβ clearance.

Similar to that found with Li, tideglusib treatment also improved recognition memory in aged (28-30 week old) *mdx* mice, whereby the treated *mdx* mice spent more time investigating the novel object when compared with vehicle treated mice (Figure 4G-H). Importantly, this was not due to any differences in the amount of movement in the arena (Figure 4I). Moreover, this could not be attributed to any differences in BACE1 activity, and thus Aβ production (Figure 4J). However, tideglusib treated *mdx* mice had greater levels of circulating serum Aβ, which may be indicative of greater vascular clearance (Figure 4K). Thus, our data shows that GSK3 inhibition in *mdx* mice improves cognitive function at both 10-12 weeks and 28-30 weeks of age. This effect was accompanied by a reduction in Aβ production and an increase in vascular clearance, with the latter imparting greater impact on cognitive function as impaired vascular Aβ clearance is known to be a key factor leading to its accumulation in AD[46].

Discussion

In the present study, we investigated the potential therapeutic benefits of GSK3 inhibition on muscle and brain health in the D2 *mdx* mouse model. GSK3 has been shown to be a viable therapeutic target for other myopathic conditions such as myotonic dystrophy type 1 (DM1)[29], limb girdle muscular dystrophy[49], amyotrophic lateral sclerosis[50,51], muscle disuse[11], and microgravity exposure[52]. To our knowledge, no study has investigated the therapeutic potential of GSK3 inhibition for DMD. However, as GSK3 inhibition not only enhances muscle health but also brain health and is an already established therapeutic strategy for various neurodegenerative diseases[53], its use for DMD could potentially improve overall well-being and quality of life. Here, our results demonstrate that treating *mdx* mice with GSK3 inhibitors, alone or in

combination with VWR, led to significant improvements in skeletal and cardiac muscle function, as well as recognition memory.

GSK3 inhibition for skeletal muscle health and metabolism

In *mdx* skeletal muscle, GSK3 inhibition can attenuate dystrophic pathology via several pathways and mechanisms including enhanced myofiber CSA and quality, reduced oxidative stress, and promotion of the oxidative fiber type program. The increase in muscle size (i.e., increase in myofiber CSA) and improvement in muscle quality (i.e., lowered necrosis) observed with GSK3 inhibition can likely contribute to improvements in muscle force production and can be acquired through various pathways. For example, GSK3 inhibition can enhance myogenic differentiation and fusion[31], which can aid in muscle regeneration in the face of constant degeneration. In addition, GSK3 inhibition can activate protein synthesis via the mTOR pathway[9]. With respect to fiber types, oxidative type I and IIA fibers are known to be more resistant to dystrophic pathology, partly because of their increased utrophin expression[13]. Utrophin provides compensatory membrane stability in the absence of dystrophin, and it can counteract dystrophic pathology. Previous studies in *mdx* mice have shown that an increase in utrophin expression attenuates disease progression[12,54,55], whereas genetic deletion of utrophin exacerbates the disease[32,33]. Consistent with this, we found that tideglusib treatment promoted the oxidative fiber type leading to an increase in utrophin expression, an attenuation of dystrophic pathology, and an increase in specific force production.

Our evidence suggests that the improvement in muscle quality and integrity offered by increasing the presence of oxidative fibers and utrophin lowers the heightened energy demands that come with muscle degeneration/regeneration cycling. Corresponding well with this, we

found that both young and aged tideglusib treated D2 *mdx* mice had lowered daily energy expenditure compared with vehicle treated *mdx* mice. Thus, GSK3 inhibition may rescue the hypermetabolic phenotype that we[39] and others[40] have previously reported. Furthermore, the hypermetabolic phenotype found in *mdx* mice has been associated with a reduction in body fat% and a significantly higher RER when compared with WT mice[40]. Again, GSK3 inhibition with tideglusib treatment reversed this effect by significantly raising body fat% and lowering RER. Though an increase in lipid supply from elevated body fat content can lower RER, the increased proportion of oxidative fibers that inherently rely less on carbohydrate sources[56,57] could also have played a role. Similar to our results with tideglusib, we also found that Li treatment lowered RER in *mdx* mice, which altogether suggests that GSK3 inhibition promotes oxidative lipid metabolism in muscle. These results may not be attributed to any improvements in mitochondrial respiration, as neither tideglusib or Li supplementation improved mitochondrial respiration at complex I or complex IV in the plantaris when compared with their respective controls (e.g., vehicle treated *mdx* mice and *mdx*-VWR mice) (Figure S8).

Moreover, both tideglusib and Li improved insulin sensitivity in *mdx* mice. In fact, we found that Li supplementation amplified the beneficial effects of VWR on insulin sensitivity. We attribute the improvement in insulin sensitivity to an enhancement in overall muscle quality, a shift towards the oxidative fibers, and the inhibition of GSK3. Skeletal muscle accounts for more than 90% of whole-body insulin-stimulated glucose removal[58] and thus decrements in muscle health can negatively impact glucose regulation. Oxidative fibers are known to be more insulin sensitive when compared with glycolytic fibers[56], and the inhibition of GSK3 has been shown to attenuate diabetes in other mouse models[59-61]. In addition to inhibiting glycogen synthase, GSK3 can phosphorylate and inactivate the insulin receptor, insulin receptor substrate, and trafficking

regulator of the glucose transporter, GLUT-4[62,63]. Thus, GSK3 acts on several pathways to limit insulin-mediated glucose disposal and as shown here, its pharmacological inhibition can have a positive effect on insulin sensitivity. These findings are clinically relevant especially when we acknowledge that DMD boys undergoing chronic glucocorticoid therapy are at increased risk for developing metabolic disorders such as insulin resistance and type 2 diabetes that ultimately further the risk of cardiovascular disease and mortality[64-66]. Glucocorticoids are the current standard of care for DMD, and while they increase the amount of ambulatory years, the presence of adverse effects such as insulin resistance can lead to early drug withdrawal[67]. Thus, future studies should determine whether GSK3 inhibitors may outperform glucocorticoids in the treatment of DMD or whether GSK3 inhibition alongside glucocorticoid treatment could be used to circumvent these adverse effects.

GSK3 inhibition and cardiac function

Given that most patients will succumb to cardiorespiratory failure, we also investigated the effects of GSK3 inhibition on cardiac muscle morphology and contractility. We first investigated the effects of tideglusib treatment on young (10-12 week old) D2 *mdx* mice. At this age and based on previous studies[35-37], the mice were not expected to have any deficits in cardiac contractility, namely %EF and %FS, as impairments in these parameters do not manifest until the mice reach 28 weeks of age. Interestingly, we found the opposite, whereby D2 *mdx* mice (vehicle and tideglusib treated) had greater %EF and %FS compared with WT controls (Table 1). This apparent increase in systolic function is consistent with a previous study using 21-week-old D2 *mdx* mice[55] and could be indicative of an age-related progression of cardiomyopathy in these mice.

In contrast with systolic function, our study was the first to examine diastolic function in young D2 *mdx* mice. Here, we show that at 10-12 weeks of age, the D2 *mdx* mice present with diastolic dysfunction that manifests as impaired relaxation (prolonged IVRT) and lowered compliance (shortened DT) when compared with WT mice (Table 1). Importantly, tideglusib treatment rescued IVRT in D2 *mdx* mice suggesting that GSK3 inhibition can improve muscle relaxation. DT is the E wave deceleration time, and is the time taken for LV and left atrial pressures to equalize during LV diastolic filling. It has been used as a valid and non-invasive marker of LV stiffness and compliance in humans[38]. In a stiffened ventricle, such as that in vehicle treated D2 *mdx* hearts, DT will be shortened; however in our study, this was lengthened and rescued with tideglusib treatment. These apparent improvements in diastolic function with GSK3 inhibition are attributed to a reduction in oxidative stress (Figure S1), and GSK3 inhibition has been shown previously to limit oxidative stress in various tissues including muscle and brain[68,69]. Oxidative stress can lead to diastolic dysfunction and lowered compliance, purportedly through negative alterations in titin which increase passive stiffness in the cardiomyocyte[70].

Similar to our tideglusib experiments, we found that Li supplementation and VWR increased DT when compared with *mdx*-SED and *mdx*-VWR groups. Thus, GSK3 inhibition afforded by tideglusib or Li may enhance compliance in D2 *mdx* hearts. However, unlike tideglusib, Li supplementation did not alter IVRT, and thus tideglusib but not Li may positively impact cardiac muscle relaxation in *mdx* mice. However, this comparison is complicated as Li supplementation was provided on top of VWR. In this respect, while we found no impairments in muscle contractility in young *mdx* mice (Table 1), we found that subjecting them to VWR for 6 weeks negatively affected %EF and %FS (Table 2). This data suggests that VWR may actually

impair cardiac contractile function in D2 *mdx* mice. Others have found that VWR had no negative impact in *mdx* mice, however, these mice were 7 months old and were on the milder C57BL/10 background[23]. Thus, we speculate that the increased level of work and contractile stress observed with cage wheel running combined with the higher degree of disease severity in D2 *mdx* mice is likely what led to the reduction in %EF and %FS (Table 2). Importantly, these reductions in %EF and %FS were not found in *mdx*-VWRLi mice, which suggests that Li supplementation in conjunction with exercise training can protect against cardiac dysfunction in the *mdx* mouse. Indeed, this result may also be due to the fact that *mdx*-VWRLi mice ran half the total distance compared with *mdx*-VWR mice.

GSK3 inhibition and cognitive function

Finally, we investigated the effects of GSK3 inhibition on cognitive function and brain biochemistry in the *mdx* mouse. In contrast with muscle, hippocampal total GSK3 levels were higher while phosphorylated GSK3 levels were lower in *mdx* mice versus WT mice. Thus, GSK3 may be overactive in the *mdx* brain and may be contributing to the cognitive decline that we and others have previously found in the *mdx* mouse[18,71-73]. In support of this, both Li supplementation and tideglusib treatment improved object recognition memory in D2 *mdx* mice leading to enhanced novel object recognition. We also examined the effects of VWR on cognitive function in *mdx* mice, as VWR has been shown to improve recognition memory in other mouse models[22-24]. However, in our hands, VWR, alone, failed to improve cognitive function in *mdx* mice. In contrast, when provided the Li supplement, we found that *mdx*-VWRLi mice had higher recognition memory when compared with both *mdx*-SED and *mdx*-VWR groups. This result is striking given that the *mdx*-VWRLi mice ran significantly less than the *mdx*-VWR mice. Thus,

GSK3 inhibition alone or along with aerobic exercise can enhance cognitive function in *mdx* mice.

Mechanistically, we explored the effects of Li supplementation and tideglusib treatment on both Aβ production via BACE1 activity, and vascular clearance by measuring serum Aβ levels. We specifically focused on Aβ production/clearance as we have shown that D2 *mdx* mice present with AD-like pathology and a shift towards amyloidogenesis[18]. Consistent with previous literature showing that GSK3 inhibition can reduce BACE1 activity and β-amyloid production to improve cognitive function in various mouse models[19,74,75], we found that *mdx*-VWRLi mice had significantly lower BACE1 activity compared with *mdx*-SED mice. However, we did not observe this effect in aged *mdx* mice treated with tideglusib as there were no differences in BACE1 activity. We believe that this might be due to an effect of age, since BACE1 activity in young (10-12 week old) *mdx* mice was significantly lower in the tideglusib group vs. the vehicle group (Figure S9).

Aside from BACE1 activity, we also examined circulating Aβ as a marker of its vascular clearance, as this is often impaired in AD[46]. Our results show that *mdx*-VWRLi mice had the greatest circulating levels of Aβ when compared with *mdx*-SED mice. Likewise, tideglusib treated *mdx* mice had significantly more serum Aβ when compared to vehicle treated mice. Altogether, this is indicative of enhanced clearance from the brain with GSK3 inhibition. The clearance of Aβ from the brain can occur enzymatically such as the insulin degrading enzyme (IDE) or neprilysin, as well as non-enzymatically by transport across the blood brain barrier and into circulation[47]. Insulin resistance and hyperinsulinemia can negatively affect both enzymatic and non-enzymatic clearance of Aβ. First, hyperinsulinemia can sequester IDE, which is not only responsible for degrading insulin, but also Aβ, ultimately allowing for Aβ oligomers to

accumulate[76,77]. Secondly, hyperinsulinemia, insulin resistance, and the ensuing hyperglycemia can negatively affect vascular clearance by causing blood brain barrier dysfunction and actually promoting the influx of Aβ back into the brain[47,78]. Given that we and others have shown that *mdx* mice exhibit drastic impairments in glucose regulation with virtually no response to insulin, it is likely that this has contributed to impairments in vascular Aβ clearance. However, since Li supplementation and tideglusib treatment improved insulin sensitivity in young and aged mice, respectively, we suspect that these improvements in glucose regulation contributed to the improvements in vascular Aβ clearance. Furthermore, oxidative stress can limit vascular Aβ clearance leading to Aβ accumulation in the brain[47]. As with our results in cardiac and skeletal muscle, we find that markers of oxidative stress are lowered in the *mdx* hippocampus after treating with both GSK3 inhibitors (Figure S10). In all, our results show that GSK3 inhibition can favourably alter the balance between Aβ production and clearance, which could contribute to the improved cognitive function in *mdx* mice.

Clinical relevance of GSK3 inhibition

We were strategic in our choice of GSK3 inhibitors for this study. Tideglusib is the most clinically advanced GSK3 inhibitor that is currently being used in Phase II clinical trials for AD, progressive supranuclear palsy, myotonic dystrophy, and autism spectrum disorders[20,21]. This is important as it could lead to a more rapid clinical integration for DMD. Furthermore, the dose that we chose to study was chosen to reflect a 600 mg dose for a 60 kg individual, which is in line with clinical trials for myotonic dystrophy[79]. Li is an already FDA-approved drug used in the treatment of bipolar disorder. Though Li toxicity has been observed in the clinical setting, these adverse events have been associated with long term therapy with relatively higher doses (above

serum Li of 1.0 mM)[43]. In the present study, we used a dose below the clinically used window of 0.5 mM – 1.0 mM serum Li concentration, which was still able to produce significant benefits on skeletal muscle specific force production, cardiac muscle diastolic and systolic function, and metabolic and cognitive health in *mdx* mice.

We chose to combine Li supplementation with VWR to determine whether the improvements in VWR previously observed in *mdx* mice[24] could be amplified with GSK3 inhibition. VWR is considered a low intensity and minimal stress model of exercise in mice, and we did not want to add any further stress with the oral gavage of tideglusib. VWR has been shown to attenuate muscle pathology in *mdx* mice and improve muscle force production partly by activating calcineurin[23,24]. Calcineurin is a Ca^{2+}-dependent phosphatase that dephosphorylates NFAT and is best known for its role in promoting the oxidative phenotype[13,80-83]. Furthermore, its activation can attenuate dystrophic pathology in *mdx* mice[12,15,84,85]. We and others have shown that GSK3 counteracts calcineurin signalling by re-phosphorylating NFAT[10,86,87], and thus the combined effects of calcineurin activation found with exercise and GSK3 inhibition could lead to additive benefits on skeletal muscle function. Consistent with this, we found that skeletal muscles from the *mdx*-VWRLi mice produced the most force compared with *mdx*-SED and *mdx*-VWR mice, and these mice also had the lowest RER – indicative of enhanced oxidative metabolism. The *mdx*-VWRLi mice were also the most-insulin sensitive, and all of these benefits were found despite running significantly less than *mdx*-VWR mice. While we do not have an explanation for these differences in exercise volume, we have also found that muscle-specific GSK3 knockdown mice run significantly less than their flox controls (Figure S11). Despite these differences in running distance, the GSK3 knockdown mice were able to attain the same level of improvement in insulin tolerance after VWR when compared with GSK3 flox control mice

(Figure S11). This reveals a clinically important aspect of GSK3 inhibition in combination with exercise. As DMD primarily affects muscle, the role of exercise in disease management has been controversial[88] and for the most part the recommended exercises have been limited to mild or moderate intensity regimes. Furthermore, those that are more affected by DMD may be unable to exercise adequately. Thus, our results showing that GSK3 inhibition with small amounts of VWR or aerobic exercise can impart benefits on muscle, brain, and metabolic health may be clinically impactful.

Conclusion

In summary, we found that treating D2 *mdx* mice with GSK3 inhibitors, tideglusib or Li, improved skeletal muscle and cardiac muscle contractility while also providing benefits to metabolic health (oxidative metabolism and glucose regulation) and cognitive function. The benefits imparted by GSK3 inhibition are multifactorial with a shift towards the oxidative fiber type, an increase in muscle size, a reduction in oxidative stress, lowered brain BACE1 activity and increased Aβ clearance as measured through serum levels. Altogether, our results have the potential to dramatically improve the quality of life of those living with DMD and should be tested in the clinical setting with either tidgelusib or low dose Li therapy.

Limitations of the study

We acknowledge several limitations to our study. First, our treatments with both tideglusib and Li were acute, and therefore, it would be important to examine the effects of long-term GSK3 inhibition. Moreover, we tested the effects of GSK3 inhibition in *mdx* mice starting at 6-8 weeks of age, which is during the initial bout of muscle degeneration[36]. We were unable to

test the effects of GSK3 inhibition in younger mice (e.g., 2-4 weeks of age) as the youngest mice available from Jackson Laboratories were 5 weeks of age. Our study is also limited in that we only tested one mouse model of DMD; and though the D2 *mdx* mouse model is more severe than the C57BL/10, future studies could examine the effects of GSK3 inhibition on the *mdx*/utrophin double knockout mice. Furthermore, when assessing mitochondrial respiration, for practical reasons we conducted our experiments in previously frozen tissue, and only analyzed the plantaris muscle. With respect to cognitive function, we only used the NORT to examine cognitive function, and there are several other tests that could be used to evaluate different types of memory and test different brain regions. We also restricted our focus to AD pathology based on our previous work; and whether this holds true for human DMD patients remain unknown. Nonetheless, and outside of AD, GSK3 inhibition has been shown to provide neuroprotection against several different diseases through several other pathways[89]. Thus, the inhibition of GSK3 could still potentially improve cognitive function in DMD patients, even if not tied to β-amyloid production. Finally, since dystrophic pathology and cardiac function worsens with age in D2 *mdx* mice[35-37], we also attempted to assess the effects of tideglusib treatment on cardiac function at 28-30 weeks of age. However, due to various experimental difficulties (e.g., maintaining adequate anesthesia and heart rate), we were only able to obtain data from a smaller sample size per group (for all groups including WT), where we saw no differences (Supplementary Table 1). Despite these limitations, our study is the first to reveal a potential universal treatment strategy for DMD focusing on both muscle and brain health to ultimately enhance quality of life.

Acknowledgements

This work was supported by an unrestricted Brock University Grant, a Canada Research Chair (Tier 2) award to VAF, and by a Brock-Niagara Validation Prototyping and Manufacturing Applied Project Grant in partnership with AMO-Pharma. BMM was supported by an NSERC USRA. SIH was supported by a NSERC Doctoral Vanier Award, JLB was supported by a CIHR CGS-D award, and BH was supported by an Ontario Graduate Scholarship. We thank Tonya Coulthard (Scintica Instruments) for her help with high frequency ultrasound analysis. We thank the animal care staff at Brock University for their assistance with animal care and handling.

Author contributions

BMM - Concept design, writing and drafting the manuscript, figure creation, data collection, data interpretation, particularly on skeletal muscle function.
ENC - Concept design, writing and drafting the manuscript, figure creation, data collection, data interpretation, particularly on cognitive function and brain biochemistry.
SIH – Concept design, writing and drafting the manuscript, figure creation, data collection, data interpretation, particularly on cardiac muscle function.
BH – Data collection, data interpretation, reviewing and revising the manuscript
JLB – Data collection, data interpretation, reviewing and revising the manuscript
MG – Data collection, data interpretation, reviewing and revising the manuscript
KCW – Data collection, data interpretation, reviewing and revising the manuscript
CJFW – Data collection, data interpretation, reviewing and revising the manuscript
LAM - Data collection, data interpretation, reviewing and revising the manuscript
BJB – Data collection, data interpretation, reviewing and revising the manuscript
ECO – Data collection, data interpretation, reviewing and revising the manuscript
AM – Data collection, data interpretation, reviewing and revising the manuscript
SS – Data collection, data interpretation, reviewing and revising the manuscript
RWB – Data collection, data interpretation, reviewing and revising the manuscript
LW – Data collection, data interpretation, reviewing and revising the manuscript
RWE - Data collection, data interpretation, reviewing and revising the manuscript
REGC – Data collection, data interpretation, reviewing and revising the manuscript
SMB - Provision of reagents and resources, reviewing and revising the manuscript
RV – Provision of reagents and resources, reviewing and revising the manuscript
BDR – Provision of reagents and resources, reviewing and revising the manuscript
JAS – Provision of reagents and resources, reviewing and revising the manuscript
AJM – Provision of reagents and resources, reviewing and revising the manuscript
REKM – Concept design, supervision, provision of reagents and resources, writing and drafting the manuscript
VAF – Concept design, supervision, provision of reagents and resources, acquiring funding, writing and drafting the manuscript

Competing interests

A portion of this project, specifically the aged (28-30 weeks) tideglusib experiments, were funded by AMO-Pharma in partnership with a Brock-Niagara Validation Prototyping and Manufacturing Applied Project Grant (1:2 monetary ratio). AMO-Pharma also provided the tideglusib for the aged tideglusib experiments.

FIGURE LEGENDS

Figure 1. Tideglusib treatment reduces muscle necrosis and improves skeletal muscle contractility (see Figure S1 and S2).

(A-C) Western blot analysis of total and serine (Ser) 9 phosphorylated GSK3β in EDL, diaphragm, and cardiac muscle homogenates from D2 WT and *mdx* mice. Analyzed with a two-way ANOVA testing the main effects of *mdx* genotype and muscle type (per muscle) (n = 6-9 per group).

(D-F) Western blot analysis of total and serine (Ser) 9 phosphorylated GSK3β in EDL, diaphragm, and cardiac muscle homogenates from vehicle and tideglusib treated D2 *mdx* mice. Analyzed with a two-way ANOVA testing the main effects of tideglusib and muscle type (per muscle) (n = 5-6 per group).

(G-H) H&E staining of EDL muscles from vehicle and tideglusib treated D2 *mdx* mice showing significant reductions in necrotic area (areas occupied by fibrosis and immune cell infiltration). Analyzed with a Student's t-test, (n = 4 per group). Scale bars are set to 200 μM.

(I) Serum creatine kinase (CK) levels are significantly elevated in vehicle treated *mdx* mice compared with tideglusib treated *mdx* mice. Analyzed with a Student's t-test, (n = 11-12 per group).

(J) Force frequency curve analysis shows that tideglusib treatment enhances EDL specific force generation. Analyzed with a two-way ANOVA where a significant interaction between frequency and tideglusib ($p < 0.0001$) was detected (n = 10-11 per group). An uncorrected Fisher's LSD test was used at the individual frequencies.

(K-M) Immunofluorescent fiber type staining show an increase in myofiber cross-sectional area (CSA) and a shift towards the oxidative (I and IIA) fibers. Analyzed with a Student's t-test (per muscle) (n = 4 per group).

(N) Utrophin *mRNA* analysis in plantaris muscles from vehicle treated and tideglusib treated D2 *mdx* mice. Analyzed with a Student's t-test (n = 7-10 per group).

All values are mean ± SEM. *p<0.05, **p<0.01.

Figure 2. Tideglusib treatment attenuates several metabolic alterations typically found in *mdx* mice (see Figure S5).

(A-B) Tideglusib lowers daily energy expenditure in young (10-12 weeks) and aged (28-30 weeks) D2 *mdx* mice. Data were analyzed with a two-way ANOVA with significant main effects denoted in the text (n = 4-5 per group).

(C-D) Tideglusib treatment did not alter cage ambulation. Data were analyzed with a two-way ANOVA with significant main effects denoted in the text (n = 4-5 per group).

(E-F) Body fat content (g) and body fat composition (% of body mass) in vehicle and tideglusib treated D2 *mdx* mice. Data were analyzed with a two-way ANOVA and a Tukey's post-hoc test used after detection of a significant interaction between tideglusib and age (n = 8-12 per group).

(G-H) Tideglusib lowers the respiratory exchange ratio (RER) in young (10-12 weeks) and aged (28-30 weeks) D2 *mdx* mice. Data were analyzed with a two-way ANOVA with significant main effects denoted in the text (n = 4-5 per group).

(I-L) Insulin tolerance tests and corresponding area-under-the-curve (AUC) analysis, baseline glucose levels and % decline in blood glucose in 28-30 week old *mdx*-vehicle and *mdx*-tidgelusib mice. Glucose traces are displayed relative to baseline glucose levels and were analyzed using a two-way ANOVA with a significant main effect of tideglusib detected (n = 8-10 per group). AUC were from the normalized traces were analyzed using a Student's t-test (n = 8-10 per group). There were no differences in baseline glucose levels.

All values are mean ± SEM. *$p<0.05$, **$p<0.01$.

Figure 3. Lithium treatment improves muscle function in *mdx* mice subjected to voluntary wheel running (see Figure S6, S7 and S9).

(A) Force frequency curve analysis in soleus muscles from WT, *mdx*-SED, *mdx*-VWR, *mdx*-VWRLi mice. Data were analyzed with a two-way ANOVA where a significant interaction between frequency and tideglusib ($p < 0.0001$) was detected (n = 8-9 per group). An uncorrected Fisher's LSD test was used at the individual frequencies.

(B) Force frequency curve analysis in EDL muscles from WT, *mdx*-SED, *mdx*-VWR, *mdx*-VWRLi mice. Data were analyzed with a two-way ANOVA where a significant interaction between frequency and tideglusib ($p = 0.0002$) was detected (n = 8-9 per group). An uncorrected Fisher's LSD test was used at the individual frequencies.

(C-D) Markers of oxidative stress, protein nitrocysteine and protein nitrotyrosine levels were measured via western blot analysis in EDL and soleus muscles from *mdx*-SED, *mdx*-VWR, and *mdx*-VWRLi mice. Data were analyzed with a two-way ANOVA where a main effect of condition was detected ($p = 0.01$ for nitrocysteine, $p = 0.04$ for nitrotyrosine), and a Tukey's post-hoc test then applied (n = 5-11 per group).

(E-F) H&E staining showing lowered muscle necrosis in *mdx*-VWRLi muscles with less signs of fibrosis and immune cell infiltration. Scale bars are set to 200 μM. Data were analyzed with a two-way ANOVA where a main effect of condition was detected ($p = 0.005$) and a Tukey's post-hoc test then applied (n = 4-6 per group). A main effect of muscle type ($p = 0.04$) was detected indicating that EDL muscle displays more muscle necrosis when compared with the soleus.

(G-J) Insulin tolerance tests and corresponding area-under-the-curve (AUC) analysis, baseline glucose levels and % decline in blood glucose in WT, *mdx*-SED, *mdx*-VWR, *mdx*-VWRLi mice. Glucose traces are displayed relative to baseline glucose levels and were analyzed using a two-way ANOVA with a Tukey's post-hoc test (n = 11 per group). AUC were from the normalized traces were analyzed using a one-way ANOVA with a Tukey's post-hoc test (n = 11 per group). There were no differences in baseline glucose levels across groups.

(K-L) Daily cage wheel distance and total distance travelled from *mdx*-VWR and *mdx*-VWRLi mice. Data were analyzed using a Student's t-test, (n = 11 per group).

All values are mean ± SEM. The number of each symbol denotes level of statistical significance. For example, *$p<0.05$, **$p<0.01$, ***$p<0.001$, ****$p<0.0001$.

Figure 4. GSK3 inhibition improves cognitive function in *mdx* mice (see Fig. S8).
(A) Total and Ser9 phosphorylated GSK3β in WT and *mdx* hippocampus. Data analyzed with a Student's t-test (n = 4 per group).
(B-D) Novel object recognition tests in *mdx*-SED, *mdx*-VWR, and *mdx*-VWRLi mice show that *mdx*-VWRLi mice have longer total investigation and novel object recognition time without any differences in total difference covered in the arena. Data analyzed with a one-way ANOVA and a Tukey's post-hoc test (n = 8-9 per group).
(E) Enzymatic BACE activity in hippocampal regions obtained from *mdx*-SED, *mdx*-VWR, and *mdx*-VWRLi mice. Data analyzed with a one-way ANOVA and a Tukey's post-hoc test (n = 4-5 per group).
(F) Serum $A\beta_{42}$ levels in *mdx*-SED, *mdx*-VWR, and *mdx*-VWRLi mice. Data analyzed with a one-way ANOVA and a Tukey's post-hoc test (n = 5-6 per group).
(G-I) Novel object recognition tests in *mdx*-vehicle and *mdx*-tideglusib mice shows that tideglusib treatment does not alter total investigation time but does increase novel object investigation time, with no differences in distance covered (m). Data analyzed with a Student's t-test (n = 7 per group).
(J) Enzymatic BACE activity in hippocampal regions obtained from *mdx*-vehicle and *mdx*-tideglusib mice. Data analyzed with a Student's t-test (n = 5-6 per group).
(K) Serum $A\beta_{42}$ levels in *mdx*-vehicle and *mdx*-tideglusib mice. Data analyzed with a Student's t-test (n = 8 per group).

Table 1. High-frequency ultrasound analysis of cardiac muscle morphology and function in in 10-12 week-old wild-type (WT), vehicle and tideglusib treated *mdx* mice (see Figure S3 and S4).

	WT	*mdx*-vehicle	*mdx*-tideglusib
LV:body mass	3.81 ± 0.12	3.81 ± 0.15	4.0 ± 0.14
LVID;d (mm)	3.59 ± 0.12	3.23 ± 0.12	3.31 ± 0.13
LVID;s (mm)	2.33 ± 0.10	1.81 ± 0.10**	1.82 ± 0.13**
RWT;d	0.58 ± 0.03	0.73 ± 0.04*	0.71 ± 0.04†
RWT;s	1.23 ± 0.08	1.90 ± 0.16**	1.88 ± 0.16**
EDV (ml)	55.1 ± 4.1	42.7 ± 4.1†	42.0 ± 2.9†
ESV (ml)	19.3 ± 1.9	10.43 ± 1.63**	10.9 ± 2.0**
SV (ml)	35.8 ± 2.8	32.3 ± 2.5	34.5 ± 2.8
HR (beats/min)	462 ± 10	469 ± 12	477 ± 11
CO (ml/min)	16.6 ± 1.5	15.1 ± 1.2	15.6 ± 1.2
EF (%)	65.0 ± 2.2	76.3 ± 1.6**	77.0 ± 2.6**
FS (%)	35.2 ± 1.7	44.2 ± 1.5**	45.4 ± 2.4**
E velocity (mm/s)	672.4 ± 30.2	615.1 ± 30.0	616.5 ± 37.9
A velocity (mm/s)	508.8 ± 26.1	433.6 ± 24.5	404.9 ± 30.6*
E/A ratio	1.3 ± 0.1	1.4 ± 0.1	1.5 ± 0.1*
DT (ms)	35.3 ± 1.2	26.3 ± 2.6*	33.9 ± 1.9$^{\#}$
IVCT (ms)	9.4 ± 1.0	9.6 ± 0.6	10.2 ± 0.8
IVRT (ms)	14.4 ± 0.5	17.4 ± 0.4***	14.9 ± 0.7$^{\#\#}$

LV:body mass, measured LV:body mass ratio; LVID;d, left ventricle internal diameter diastole; LVID;s, left ventricle internal diameter systole; RWT;d, relative wall thickness diastole; RWT;s, relative wall thickness systole; EDV, end-diastolic volume; ESV, end-systolic volume; SV, stroke volume, EF; ejection fraction; FS, fractional shortening, CO, cardiac output; HR, heart rate, DT, deceleration time; IVCT, isovolumic contraction time; IVRT, isovolumic relaxation time. A one-way ANOVA with a Tukey's post-hoc test was used; vs. WT, $^{\dagger}p < 0.10$, $*p < 0.05$, $**p < 0.01$; vs. *mdx*-vehicle, $^{\#}p < 0.05$, $^{\#\#}p < 0.01$; using a One-way ANOVA with a Tukey's post-hoc test, (n=10-12 per group except for LV:body mass, n = 6 per group).

Table 2. High-frequency ultrasound analysis of cardiac muscle morphology and function in age-matched *mdx* -SED, *mdx*-VWR, and *mdx*-VWRLi mice.

	***mdx*-SED**	***mdx*-VWR**	***mdx*-VWRLi**
LVID;d (mm)	3.63 ± 0.14	3.82 ± 0.10	3.9 ± 0.10
LVID;s (mm)	2.37 ± 0.22	2.84 ± 0.15	2.78 ± 0.17
RWT;d	0.70 ± 0.08	0.68 ± 0.06	0.69 ± 0.05
RWT;s	1.38 ± 0.21	1.02 ± 0.07	1.17 ± 0.18
EDV (µL)	56.7 ± 5.1	63.8 ± 4.1	69.6 ± 3.3
ESV (µL)	22.6 ± 5.1	31.5 ± 3.8	30.1 ± 4.0
SV (µL)	34.2 ± 2.2	32.4 ± 3.0	39.5 ± 2.3
EF (%)	67.8 ± 4.2	51.2 ± 4.4*	57.3 ± 4.5
FS (%)	38.3 ± 3.5	26.1 ± 2.8*	32.3 ± 3.5
E velocity (mm/s)	364.1 ± 28.8	403.4 ± 38.4	399.1 ± 36.9
A velocity (mm/s)	270.0 ± 24.5	283.1 ± 27.4	285.9 ± 15.7
E/A ratio	1.40 ± 0.09	1.45 ± 0.07	1.39 ± 0.08
DT (ms)	30.6 ± 2.5##	30.6 ± 2.4##	44.3 ± 3.4
IVCT (ms)	15.0 ± 1.1	15.0 ± 1.2	14.7 ± 0.3
IVRT (ms)	25.9 ± 0.5	27.1 ± 1.4	28.8 ± 0.7

LVID;d, left ventricle internal diameter diastole; LVID;s, left ventricle internal diameter systole; RWT;d, relative wall thickness diastole; RWT;s, relative wall thickness systole; EDV, end-diastolic volume; ESV, end-systolic volume; SV, stroke volume, EF; ejection fraction; FS, fractional shortening; DT, deceleration time; IVCT, isovolumic contraction time; IVRT, isovolumic relaxation time. A one-way ANOVA with a Tukey's post-hoc test was used; * vs. *mdx*-SED $p<0.05$, ##vs. *mdx*-VWRLi, $p < 0.01$. All values are mean ± SEM (n = 7-11).

STAR METHODS

RESOURCE AVAILABILITY

Lead contact

Further information and requests for resources and reagents should be directed to and will be fulfilled by the lead contact, Val A. Fajardo (vfajardo@brocku.ca).

Materials availability

This study did not generate new unique reagents.

Data and code availability

- All data reported in this paper will be shared by the lead contact upon request.
- This paper does not report original code.
- Any additional information required to reanalyze the data reported in this paper is available from the lead contact upon request.

EXPERIMENTAL MODELS AND SUBJECT DETAILS

Mice and Design

DBA/2J (D2)-*mdx* (stock #001801) and D2 WT (stock #000671) were ordered from Jackson Laboratories at 5-6 weeks of age. For the aged tideglusib experiments, *mdx* mice were ordered from Jackson Laboratories at 7-9 weeks of age with treatment starting at 24-26 weeks of age. Muscle-specific GSK3 KD mice were generated in our lab using cryorecovered GSK3 α and β floxed mice[90]. All mice were housed in Brock University's Animal Facility, in an environmentally controlled room with a standard 12:12 hour light-dark cycle and allowed access to food and water *ad libitum*.

Tideglusib treatment

D2 *mdx* mice were treated with tideglusib at a dose of 10mg/kg/day via oral gavage, whereas a separate vehicle group of D2 *mdx* mice were given 26% peg400, 15% Chremaphor EL and water[29] for 5 days per week. A separate group of WT mice were also housed simultaneously to serve as a healthy reference control. Young D2 *mdx* mice were treated for a period of 2-4 weeks to allow for a variety of *in vivo* measures to be conducted. A subset of D2 *mdx* (vehicle and tideglusib) mice were euthanized after 2 weeks to examine GSK3 activation, fiber type composition and necrosis via histological staining (n = 5-6 per group). The remaining mice were treated for an additional two weeks to conduct several *in vivo* measures and additional biochemical (SERCA function and western blotting) and histological measures (cardiac histology) (n = 10-12 per group).

Voluntary wheel running and Li supplementation

D2 *mdx* mice were randomly divided into 3 groups: 1) *mdx*-SED, 2) *mdx*-VWR, and 3) *mdx*-VWRLi (n = 11 per group). The VWR groups were provided with a cage wheel for 6 weeks and all mice were housed in the Techniplast DVC80 with GYM500 software to track cage wheel distance travelled 24/7. The Li-fed *mdx* mice were provided lithium chloride (50 mg/kg/day) in their drinking water with 2 water changes per week for the entire duration of the study.

METHOD DETAILS

RER analysis

Mice were housed in the Promethion Metabolic Screening System for a period of 48 hours to track fuel utilization. The cages are connected to a flow regulator and O_2 and CO_2 gas

analyzers which measure the volume of carbon dioxide produced (VCO_2) and the volume of oxygen consumed (VO_2). Respiratory exchange ratio (RER) was calculated as VCO_2 divided by VO_2.

Insulin tolerance test

Insulin tolerance testing was performed as previously described[90]. Briefly, concentrations of blood glucose were determined by sampling blood from the tail vein at 0, 15, 30, 60, and 120 min following the IP insulin injection (0.5 U/kg) with the use of a hand-held glucometer (Freestyle Lite; Abbott). Plots of the average changes in plasma glucose over time were made for each group, and the average total area under the curve was calculated. Area under the curve is presented in mmol/l × time, and baseline values are set to X = 0. The % decline in blood glucose was calculated by taking the largest drop in blood glucose throughout the 120 min divided by the baseline glucose levels (timepoint 0).

High frequency ultrasound

Mice were subjected to high frequency ultrasound analysis using a Prospect T1 high frequency ultrasound (S-Sharp, Taiwan). Short axis M-mode imaging was used to calculate systolic function, including the LVID, RWT, EDV, ESV, SV, %EF, %FS, and CO. PW doppler of the mitral valve inflow, from an apical 4-chamber view, was used to assess diastolic function, specifically measuring E velocity, A velocity, deceleration time, IVRT and IVCT. Measurements were taken at a maintained heart rate of 400-550 bpm.

Novel object recognition test

Novel object recognition tests were performed as previously described[18] but modified so that data analysis was automated with DeepLabCut[91] and custom MATLAB scripts (v2022a, MathWorks Inc.). The mice were habituated to the arena the day prior to testing where they could explore freely for 10 minutes. Following the habituation, the mice were placed in the arenas with two identical objects in the bottom corners and were left to explore for 10-minutes. The mice were then returned to their home cages for a 60-minute intertrial retention delay. Next, the mice were returned to the arena where one of the familiar objects was replaced by a novel object and they were given 10-minutes to investigate. Extracted outcomes included the time spent at trained and untrailed targets (reflected as a percentage of the trail duration), the total distance travelled by each mouse, and the mean speed at which the mouse navigated the arena.

Sample and tissue collection

All mice were euthanized via exsanguination under general anesthetic (vaporized isoflurane) and their tissues and blood were collected. Blood was spun at 5000 x g for 8 minutes (4˚C) and serum was collected and stored at -80˚C. Extensor digitorum longus (EDL), soleus, plantaris, diaphragm, gastrocnemius, quadriceps, cardiac muscles, and hippocampal brain regions were isolated and stored at -80˚C for further analysis.

Isolated muscle contractility

Soleus and EDL muscles were carefully dissected and mounted onto an Aurora Scientific contractile apparatus (model 305B&701B) to assess muscle force production and fatigue as previously described[10]. Muscles were subjected to a force-frequency protocol (1–160 Hz). For data analyses, peak isometric force amplitude (mN) was determined across the range of

stimulation frequencies. Peak isometric force was then normalized to muscle cross-sectional area (CSA), which was calculated using the following formula: CSA = m/l*d*(L_f/L_o), where m, muscle mass (mg); l, muscle length (mm); d, mammalian skeletal muscle density (1.06 mg/mm^3)[92]. Lf/Lo is the fiber length-to-muscle length ratio (0.44 for the EDL and 0.71 for the soleus)[93].

Serum CK, Li, BACE1, and Aβ_{42} analysis

Serum creatine kinase (CK) activity was measured with a M2 Molecular Device plate reader and a commercially available assay (Cat. #C7522, Pointe Scientific Inc., Canton, MI, USA) fitted onto a 96-well plate and calibrated with a standard curve of purified creatine kinase (Sigma, Oakville, ON, Canada, Cat. 10127566001). Serum Li analysis in the *mdx*-VWRLi mice were measured using the commercially available kit (ab235613, Abcam). BACE1 activity was measured using the commercially available kit (ab65357, Abcam). Serum Aβ_{42} content was measured using the commercially available kit (KMB3441, Life Technologies).

Immunofluorescent fiber typing

Fiber typing was accomplished through immunofluorescent staining of myosin heavy chain (MHC) isoforms in 10 μm sections of the EDL and soleus muscles as previously described[94]. Slides were imaged using a BioTek Cytation 5 Multimode Plate Reader at 10x magnification using auto-exposure settings for three filters: DAPI, GFP, and Texas Red. Images were then stitched, processed and saved using the Gen5 image processing functions, and then analyzed using ImageJ (NIH) software to estimate fiber type composition and CSA.

Histological assessment

For EDL and soleus muscles, necrosis was measured using Hematoxylin and Eosin (H&E) staining of EDL muscle samples. All slides were imaged using a BioTek Cytation 5 Multimode Plate Reader. All images were acquired using 10x magnification using auto-exposure settings for the Colour Brightfield setting. Images were then saved and then analyzed using ImageJ (NIH) software to estimate necrotic area. This was done by calculating the total surface area of the muscle, then calculating the sum of the area of all necrosis (areas occupied by collagen and immune cell infiltration) within the sample. This total necrosis was then divided by the total area of the sample.

For cardiac histology, hearts were isolated and fixed in 10% formalin for 72hrs then transferred to 70% (v/v) ethanol until being embedded in paraffin wax (n = 5 per group). Slices 10 μm in size were affixed to vectabond-treated slides and stained with Gamori trichrome stain with muscle tissues stained red, nuclei stained black and fibrotic tissue stained blue. Images were taken at 20x magnification at the apex, base and mid-region of the left ventricle of the heart (4-6 images per area). Images were analyzed using ImageJ software (US National Institutes of Health) to identify % fibrosis by measuring total blue area (fibrotic tissue) divided by total red area (muscle tissue) x 100%.

Western blotting

Western blotting was done to assess protein levels of GSK3β, Ser9 phosphorylated GSK3β, and total protein nitration (nitrotyrosine) and nitrosylation (nitrocysteine). Standard SDS-PAGE was performed with BioRad 7-12% TGX gels (4561086; BioRad, Hercules, CA, USA) and polyvinylidine difluoride (PVDF) membranes were used for all proteins (BioRad). All protein blots were blocked with Everyblot buffer (#12010020, BioRad) for 10 min at room

temperature and incubated with primary and corresponding secondary antibodies (Supplementary Table 1) prior to imaging with a BioRad ChemiDoc Imager with Immobilon ECL Ultra Western HRP Substrate (WBKLS0500, Sigma-Aldrich). Images were analyzed using BioRad ImageLab software (BioRad) and were normalized to total protein analyzed on a Ponceau stain or GAPDH.

mRNA analysis

mRNA analyses for utrophin (forward, GGGGAAGATGTGAGAGATTT; reverse, GTGTGGTGAGGAGATACGAT) was accomplished by homogenizing plantaris (*mdx*-vehicle and *mdx*-tideglusib) and quadriceps (*mdx*-SED, *mdx*-VWR, *mdx*-LiVWR) samples with 1mL of TRIzol. A commercially available Qiagen RNeasy kit (Quiagen, Hilden, Germany, ID #74104) and a DNase Max kit (Quiagen, Hilden, Germany, D #15200-50) was then used to isolate RNA. This was then quantified using a NanoVue Plus spectrophotometer (Biochrom Ltd., Cambridge, UK), followed by the use of EcoDry RNA to cDNA (Takara Bio Inc., Kusatsu, Shiga, Japan, ID #639547) reaction tubes and a SimpliAmp Thermal Cylinder (ThermoFisher, MA, USA, ID #A24811) to facilitate the generation of cDNA. Diluted cDNA was then analyzed using a qPCR reaction 96-well plate and the StepOnePlus Real-Time PCR System (ThermoFisher, MA, USA, ID #4376600). Threshold cycle (Ct) values were recorded, and data were analyzed using the ΔΔCt method and reported as a fold-change (2ΔCt), using expression of the Gapdh housekeeping gene as a reference (forward, CGGTGCTGAGTATGTCGTGGAGTC; reverse, GGGGCTAAGCAGTTGGTGGTG; IDT).

SERCA function

SERCA function was assessed in diaphragm and cardiac muscle homogenates using an oxalate-supported Ca^{2+} uptake fluorometric assay and an ionophore (A23187, Sigma Aldrich)-supported spectrophotometric SERCA activity assay, both fitted onto a 96-well plate using an M2 MultiMode plate reader (Molecular Devices) as previously described[95,96]. For both Ca^{2+} uptake and SERCA activity, rates were normalized to total protein obtained from a BCA assay.

Mitochondrial respiration

Respirometry analysis of previously frozen tissue homogenates, along with the corresponding tissue homogenisation, was performed based on the method described in Acin-Perez et al., 2020[97] & Osto et al., 2020[98]. Plantaris muscle tissue samples were isolated, snap frozen, and stored at -80°C. Tissue samples were weighed and homogenised in ice-cold MAS (1x, pH 7.4, consisting of 70 mM sucrose, 220 mM mannitol, 5 mM KH_2PO_4, 5 mM $MgCL_2$, 1 mM EGTA, 2 mM HEPES) supplemented with 0.25 mg/mL collagenase type II (homogenisation buffer) at a ratio of 500 µL per 10 mg tissue. Homogenisation was performed on ice using a pre-chilled glass-glass Dounce homogeniser with 20 strokes. Samples were then incubated at 37°C for 30 min to aid in collagen digestion and then centrifuged at 2000 x g for 3 min at 4°C. The resulting supernatant (tissue homogenate) was stored at -80°C for downstream use. Protein concentration was determined using the BCA assay that included BSA standards prepared in homogenisation buffer.

Respirometry assays were performed using an Agilent Seahorse XFe24 Analyzer. Tissue homogenates (10 µg) were loaded into Seahorse XFe24 microplate wells in 60 µL of MAS. The loaded plate was centrifuged at 2000 x g for 5 minutes with a low break setting (deceleration

speed of 3/9 on Qiagen 4-15C plate centrifuge) and an additional 390 µL of pre-warmed (37°C) MAS containing 10 µg/µL cytochrome c (respiration buffer) was carefully added to each well. Compound injections were prepared in MAS and injected as follows (75 µL injection per port): NADH (1.43 mM) at port A, Antimycin A (4 µM) at port B, TMPD + Ascorbate (0.55 mM and 1.11 mM, respectively) at port C, and sodium azide (50 mM) at port D. Mixing steps and measurement steps consisted of 30 seconds and 4 minutes, respectively. From the oxygen consumption rate (OCR) data, the following parameters were calculated: i) Respiratory capacity through Complex I = OCR_{NADH} minus $OCR_{Antimycin\ A}$, and ii) Respiratory capacity through Complex IV = $OCR_{TMPD+Ascorbate}$ minus OCR_{Azide}.

Dichlorofluorescein (DCF) assay

DCF assays were performed in hippocampal regions from the D2 WT and *mdx* brain to assess total reactive oxygen species (ROS) levels as briefly described [99]. Tissue homogenates (25 ul) were incubated with 5 µM 2′,7′-Dichlorofluorescin diacetate (D6883, Sigma) for 10 minutes at 37°C. Fluorescence was measured using an M2 Multimode Plate reader (emission: 490 nm and excitation: 525 nm) and was normalized to total protein obtained from a BCA assay.

Ethics statement

All animal procedures were approved by the Brock University Animal Care and Utilization Committee (file #17-06-03, 20-07-01, and 22-04-01) and were carried out in accordance with the Canadian Council on Animal Care guidelines.

QUANTIFICATION AND STATISTICAL ANALYSIS

Statistical analysis

Statistical comparisons were made using a Student's t-test, a one-way or two-way ANOVA with a Tukey's or Fisher's LSD post-hoc test where appropriate. All statistical analysis were done using Graphpad Prism 8 software. A Welch's t-test or ANOVA were used in cases where variability between groups significantly differed. Statistical significance was set to a $p \leq 0.05$. All values are presented as means ± SEM.

References

1. Mah, J.K., Korngut, L., Dykeman, J., Day, L., Pringsheim, T., and Jette, N. (2014). A systematic review and meta-analysis on the epidemiology of Duchenne and Becker muscular dystrophy. Neuromuscul Disord *24*, 482-491. 10.1016/j.nmd.2014.03.008.
2. Falzarano, M.S., Scotton, C., Passarelli, C., and Ferlini, A. (2015). Duchenne Muscular Dystrophy: From Diagnosis to Therapy. Molecules *20*, 18168-18184. 10.3390/molecules201018168.
3. Laviola, M., Priori, R., D'Angelo, M.G., and Aliverti, A. (2018). Assessment of diaphragmatic thickness by ultrasonography in Duchenne muscular dystrophy (DMD) patients. PLoS One *13*, e0200582. 10.1371/journal.pone.0200582.
4. Cotton, S., Voudouris, N.J., and Greenwood, K.M. (2001). Intelligence and Duchenne muscular dystrophy: full-scale, verbal, and performance intelligence quotients. Dev Med Child Neurol *43*, 497-501. 10.1017/s0012162201000913.
5. Dorman, C., Hurley, A.D., and D'Avignon, J. (1988). Language and learning disorders of older boys with Duchenne muscular dystrophy. Dev Med Child Neurol *30*, 316-327. 10.1111/j.1469-8749.1988.tb14556.x.
6. Beurel, E., Grieco, S.F., and Jope, R.S. (2015). Glycogen synthase kinase-3 (GSK3): regulation, actions, and diseases. Pharmacol Ther *148*, 114-131. 10.1016/j.pharmthera.2014.11.016.
7. Wang, H., Brown, J., and Martin, M. (2011). Glycogen synthase kinase 3: a point of convergence for the host inflammatory response. Cytokine *53*, 130-140. 10.1016/j.cyto.2010.10.009.
8. Leroy, K., and Brion, J.P. (1999). Developmental expression and localization of glycogen synthase kinase-3beta in rat brain. J Chem Neuroanat *16*, 279-293. 10.1016/s0891-0618(99)00012-5.
9. Mirzoev, T.M., Sharlo, K.A., and Shenkman, B.S. (2021). The Role of GSK-3β in the Regulation of Protein Turnover, Myosin Phenotype, and Oxidative Capacity in Skeletal Muscle under Disuse Conditions. Int J Mol Sci *22*, 5081. 10.3390/ijms22105081.
10. Whitley, K.C., Hamstra, S.I., Baranowski, R.W., Watson, C.J.F., MacPherson, R.E.K., MacNeil, A.J., Roy, B.D., Vandenboom, R., and Fajardo, V.A. (2020). GSK3 inhibition with low dose lithium supplementation augments murine muscle fatigue resistance and specific force production. Physiol Rep *8*, e14517. 10.14814/phy2.14517.
11. Pansters, N.A., Schols, A.M., Verhees, K.J., de Theije, C.C., Snepvangers, F.J., Kelders, M.C., Ubags, N.D., Haegens, A., and Langen, R.C. (2015). Muscle-specific GSK-3beta ablation accelerates regeneration of disuse-atrophied skeletal muscle. Biochim Biophys Acta *1852*, 490-506. 10.1016/j.bbadis.2014.12.006.
12. Chakkalakal, J.V., Harrison, M.A., Carbonetto, S., Chin, E., Michel, R.N., and Jasmin, B.J. (2004). Stimulation of calcineurin signaling attenuates the dystrophic pathology in mdx mice. Hum Mol Genet *13*, 379-388. 10.1093/hmg/ddh037.
13. Chakkalakal, J.V., Stocksley, M.A., Harrison, M.A., Angus, L.M., Deschenes-Furry, J., St-Pierre, S., Megeney, L.A., Chin, E.R., Michel, R.N., and Jasmin, B.J. (2003). Expression of utrophin A mRNA correlates with the oxidative capacity of skeletal muscle fiber types and is regulated by calcineurin/NFAT signaling. Proc Natl Acad Sci U S A *100*, 7791-7796. 10.1073/pnas.0932671100.
14. Fajardo, V.A., Chambers, P.J., Juracic, E.S., Rietze, B.A., Gamu, D., Bellissimo, C., Kwon, F., Quadrilatero, J., and Russell Tupling, A. (2018). Sarcolipin deletion in mdx

mice impairs calcineurin signalling and worsens dystrophic pathology. Hum Mol Genet. 10.1093/hmg/ddy302.
15. Chakkalakal, J.V., Michel, S.A., Chin, E.R., Michel, R.N., and Jasmin, B.J. (2006). Targeted inhibition of Ca2+ /calmodulin signaling exacerbates the dystrophic phenotype in mdx mouse muscle. Hum Mol Genet *15*, 1423-1435. 10.1093/hmg/ddl065.
16. Ning, H., Ren, H., Zhao, Y., Yin, H., Gan, Z., Shen, Y., and Yu, Y. (2022). Targeting the DP2 receptor alleviates muscle atrophy and diet-induced obesity in mice through oxidative myofiber transition. J Cachexia Sarcopenia Muscle. 10.1002/jcsm.13136.
17. Cohen, P., and Goedert, M. (2004). GSK3 inhibitors: development and therapeutic potential. Nat Rev Drug Discov *3*, 479-487. 10.1038/nrd1415.
18. Hayward, G.C., Caceres, D., Copeland, E.N., Baranowski, B.J., Mohammad, A., Whitley, K.C., Fajardo, V.A., and MacPherson, R.E.K. (2022). Characterization of Alzheimer's disease-like neuropathology in Duchenne's muscular dystrophy using the DBA/2J mdx mouse model. FEBS Open Bio *12*, 154-162. 10.1002/2211-5463.13317.
19. Ly, P.T., Wu, Y., Zou, H., Wang, R., Zhou, W., Kinoshita, A., Zhang, M., Yang, Y., Cai, F., Woodgett, J., and Song, W. (2013). Inhibition of GSK3β-mediated BACE1 expression reduces Alzheimer-associated phenotypes. J Clin Invest *123*, 224-235. 10.1172/jci64516.
20. Khan, I., Tantray, M.A., Alam, M.S., and Hamid, H. (2017). Natural and synthetic bioactive inhibitors of glycogen synthase kinase. Eur J Med Chem *125*, 464-477. 10.1016/j.ejmech.2016.09.058.
21. Noori, M.S., Bhatt, P.M., Courreges, M.C., Ghazanfari, D., Cuckler, C., Orac, C.M., McMills, M.C., Schwartz, F.L., Deosarkar, S.P., Bergmeier, S.C., et al. (2019). Identification of a novel selective and potent inhibitor of glycogen synthase kinase-3. Am J Physiol Cell Physiol *317*, C1289-c1303. 10.1152/ajpcell.00061.2019.
22. Vecchio, L.M., Meng, Y., Xhima, K., Lipsman, N., Hamani, C., and Aubert, I. (2018). The Neuroprotective Effects of Exercise: Maintaining a Healthy Brain Throughout Aging. Brain Plast *4*, 17-52. 10.3233/bpl-180069.
23. Ferry, A., Benchaouir, R., Joanne, P., Peat, R.A., Mougenot, N., Agbulut, O., and Butler-Browne, G. (2015). Effect of voluntary physical activity initiated at age 7 months on skeletal hindlimb and cardiac muscle function in mdx mice of both genders. Muscle Nerve *52*, 788-794. 10.1002/mus.24604.
24. Delacroix, C., Hyzewicz, J., Lemaitre, M., Friguet, B., Li, Z., Klein, A., Furling, D., Agbulut, O., and Ferry, A. (2018). Improvement of Dystrophic Muscle Fragility by Short-Term Voluntary Exercise through Activation of Calcineurin Pathway in mdx Mice. Am J Pathol *188*, 2662-2673. 10.1016/j.ajpath.2018.07.015.
25. Lott, D.J., Taivassalo, T., Cooke, K.D., Park, H., Moslemi, Z., Batra, A., Forbes, S.C., Byrne, B.J., Walter, G.A., and Vandenborne, K. (2021). Safety, feasibility, and efficacy of strengthening exercise in Duchenne muscular dystrophy. Muscle Nerve *63*, 320-326. 10.1002/mus.27137.
26. Zelikovich, A.S., Quattrocelli, M., Salamone, I.M., Kuntz, N.L., and McNally, E.M. (2019). Moderate exercise improves function and increases adiponectin in the mdx mouse model of muscular dystrophy. Scientific Reports *9*, 5770. 10.1038/s41598-019-42203-z.
27. MacAulay, K., and Woodgett, J.R. (2008). Targeting glycogen synthase kinase-3 (GSK-3) in the treatment of Type 2 diabetes. Expert Opin Ther Targets *12*, 1265-1274. 10.1517/14728222.12.10.1265.

28. Balasubramaniam, M., Mainali, N., Bowroju, S.K., Atluri, P., Penthala, N.R., Ayyadevera, S., Crooks, P.A., and Shmookler Reis, R.J. (2020). Structural modeling of GSK3β implicates the inactive (DFG-out) conformation as the target bound by TDZD analogs. Scientific Reports *10*, 18326. 10.1038/s41598-020-75020-w.
29. Jones, K., Wei, C., Iakova, P., Bugiardini, E., Schneider-Gold, C., Meola, G., Woodgett, J., Killian, J., Timchenko, N.A., and Timchenko, L.T. (2012). GSK3beta mediates muscle pathology in myotonic dystrophy. J Clin Invest *122*, 4461-4472. 10.1172/JCI64081.
30. Armagan, G., Sevgili, E., Gürkan, F.T., Köse, F.A., Bilgiç, T., Dagcı, T., and Saso, L. (2019). Regulation of the Nrf2 Pathway by Glycogen Synthase Kinase-3β in MPP+-Induced Cell Damage. Molecules *24*. 10.3390/molecules24071377.
31. Kurgan, N., Whitley, K.C., Maddalena, L.A., Moradi, F., Stoikos, J., Hamstra, S.I., Rubie, E.A., Kumar, M., Roy, B.D., Woodgett, J.R., et al. (2019). A Low-Therapeutic Dose of Lithium Inhibits GSK3 and Enhances Myoblast Fusion in C2C12 Cells. Cells *8*. 10.3390/cells8111340.
32. Deconinck, A.E., Rafael, J.A., Skinner, J.A., Brown, S.C., Potter, A.C., Metzinger, L., Watt, D.J., Dickson, J.G., Tinsley, J.M., and Davies, K.E. (1997). Utrophin-dystrophin-deficient mice as a model for Duchenne muscular dystrophy. Cell *90*, 717-727.
33. Grady, R.M., Teng, H., Nichol, M.C., Cunningham, J.C., Wilkinson, R.S., and Sanes, J.R. (1997). Skeletal and cardiac myopathies in mice lacking utrophin and dystrophin: a model for Duchenne muscular dystrophy. Cell *90*, 729-738.
34. Angus, L.M., Chakkalakal, J.V., Mejat, A., Eibl, J.K., Belanger, G., Megeney, L.A., Chin, E.R., Schaeffer, L., Michel, R.N., and Jasmin, B.J. (2005). Calcineurin-NFAT signaling, together with GABP and peroxisome PGC-1{alpha}, drives utrophin gene expression at the neuromuscular junction. Am J Physiol Cell Physiol *289*, C908-917. 10.1152/ajpcell.00196.2005.
35. Coley, W.D., Bogdanik, L., Vila, M.C., Yu, Q., Van Der Meulen, J.H., Rayavarapu, S., Novak, J.S., Nearing, M., Quinn, J.L., Saunders, A., et al. (2016). Effect of genetic background on the dystrophic phenotype in mdx mice. Hum Mol Genet *25*, 130-145. 10.1093/hmg/ddv460.
36. Hammers, D.W., Hart, C.C., Matheny, M.K., Wright, L.A., Armellini, M., Barton, E.R., and Sweeney, H.L. (2020). The D2.mdx mouse as a preclinical model of the skeletal muscle pathology associated with Duchenne muscular dystrophy. Sci Rep *10*, 14070. 10.1038/s41598-020-70987-y.
37. van Putten, M., Putker, K., Overzier, M., Adamzek, W.A., Pasteuning-Vuhman, S., Plomp, J.J., and Aartsma-Rus, A. (2019). Natural disease history of the D2-mdx mouse model for Duchenne muscular dystrophy. FASEB J *33*, 8110-8124. 10.1096/fj.201802488R.
38. Little, W.C., Ohno, M., Kitzman, D.W., Thomas, J.D., and Cheng, C.P. (1995). Determination of left ventricular chamber stiffness from the time for deceleration of early left ventricular filling. Circulation *92*, 1933-1939. 10.1161/01.cir.92.7.1933.
39. Cleverdon, R.E.G., Braun, J.L., Geromella, M.S., Whitley, K.C., Marko, D.M., Hamstra, S.I., Roy, B.D., MacPherson, R.E.K., and Fajardo, V.A. (2022). Sarco(endo)plasmic reticulum Ca(2+)-ATPase function is impaired in skeletal and cardiac muscles from young DBA/2J mdx mice. iScience *25*, 104972. 10.1016/j.isci.2022.104972.
40. Strakova, J., Kamdar, F., Kulhanek, D., Razzoli, M., Garry, D.J., Ervasti, J.M., Bartolomucci, A., and Townsend, D. (2018). Integrative effects of dystrophin loss on

metabolic function of the mdx mouse. Scientific Reports *8*, 13624. 10.1038/s41598-018-31753-3.
41. Podkalicka, P., Mucha, O., Kaziród, K., Szade, K., Stępniewski, J., Ivanishchuk, L., Hirao, H., Pośpiech, E., Józkowicz, A., Kupiec-Weglinski, J.W., et al. (2022). miR-378 affects metabolic disturbances in the mdx model of Duchenne muscular dystrophy. Scientific Reports *12*, 3945. 10.1038/s41598-022-07868-z.
42. Kim, Y.J., Kim, H.J., Lee, W.J., and Seong, J.K. (2020). A comparison of the metabolic effects of treadmill and wheel running exercise in mouse model. Laboratory Animal Research *36*, 3. 10.1186/s42826-019-0035-8.
43. Hamstra, S.I., Roy, B.D., Tiidus, P., MacNeil, A.J., Klentrou, P., MacPherson, R.E.K., and Fajardo, V.A. (2022). Beyond its psychiatric use: the benefits of low dose lithium supplementation. Curr Neuropharmacol. 10.2174/1570159x20666220302151224.
44. Reitz, C., Brayne, C., and Mayeux, R. (2011). Epidemiology of Alzheimer disease. Nat Rev Neurol *7*, 137-152. 10.1038/nrneurol.2011.2.
45. Harman, D. (2006). Alzheimer's disease pathogenesis: role of aging. Ann N Y Acad Sci *1067*, 454-460. 10.1196/annals.1354.065.
46. Mawuenyega, K.G., Sigurdson, W., Ovod, V., Munsell, L., Kasten, T., Morris, J.C., Yarasheski, K.E., and Bateman, R.J. (2010). Decreased clearance of CNS beta-amyloid in Alzheimer's disease. Science *330*, 1774. 10.1126/science.1197623.
47. Winkler, E.A., Sagare, A.P., and Zlokovic, B.V. (2014). The pericyte: a forgotten cell type with important implications for Alzheimer's disease? Brain Pathol *24*, 371-386. 10.1111/bpa.12152.
48. Salam, E.A., Abdel-Meguid, I.E., Shatla, R., and Korraa, S. (2014). Evaluation of neural damage in Duchenne muscular dystrophy patients. Acta Myol *33*, 13-18.
49. Findlay, A.R., Bengoechea, R., Pittman, S.K., Chou, T.F., True, H.L., and Weihl, C.C. (2019). Lithium chloride corrects weakness and myopathology in a preclinical model of LGMD1D. Neurol Genet *5*, e318. 10.1212/NXG.0000000000000318.
50. Feng, H.L., Leng, Y., Ma, C.H., Zhang, J., Ren, M., and Chuang, D.M. (2008). Combined lithium and valproate treatment delays disease onset, reduces neurological deficits and prolongs survival in an amyotrophic lateral sclerosis mouse model. Neuroscience *155*, 567-572. 10.1016/j.neuroscience.2008.06.040.
51. Group, U.K.-L.S., Morrison, K.E., Dhariwal, S., Hornabrook, R., Savage, L., Burn, D.J., Khoo, T.K., Kelly, J., Murphy, C.L., Al-Chalabi, A., et al. (2013). Lithium in patients with amyotrophic lateral sclerosis (LiCALS): a phase 3 multicentre, randomised, double-blind, placebo-controlled trial. Lancet Neurol *12*, 339-345. 10.1016/S1474-4422(13)70037-1.
52. Baranowski, R.W., Braun, J.L., Hockey, B.L., Yumol, J.L., Geromella, M.S., Watson, C.J.F., Kurgan, N., Messner, H.N., Whitley, K.C., MacNeil, A.J., et al. (2023). Toward countering muscle and bone loss with spaceflight: GSK3 as a potential target. iScience *26*, 107047. https://doi.org/10.1016/j.isci.2023.107047.
53. Rockenstein, E., Torrance, M., Adame, A., Mante, M., Bar-on, P., Rose, J.B., Crews, L., and Masliah, E. (2007). Neuroprotective effects of regulators of the glycogen synthase kinase-3beta signaling pathway in a transgenic model of Alzheimer's disease are associated with reduced amyloid precursor protein phosphorylation. J Neurosci *27*, 1981-1991. 10.1523/JNEUROSCI.4321-06.2007.

54. Tinsley, J., Deconinck, N., Fisher, R., Kahn, D., Phelps, S., Gillis, J.M., and Davies, K. (1998). Expression of full-length utrophin prevents muscular dystrophy in mdx mice. Nat Med *4*, 1441-1444. 10.1038/4033.
55. Kennedy, T.L., Guiraud, S., Edwards, B., Squire, S., Moir, L., Babbs, A., Odom, G., Golebiowski, D., Schneider, J., Chamberlain, J.S., and Davies, K.E. (2018). Micro-utrophin Improves Cardiac and Skeletal Muscle Function of Severely Affected D2/mdx Mice. Mol Ther Methods Clin Dev *11*, 92-105. 10.1016/j.omtm.2018.10.005.
56. Schiaffino, S., and Reggiani, C. (2011). Fiber types in mammalian skeletal muscles. Physiol Rev *91*, 1447-1531. 10.1152/physrev.00031.2010

91/4/1447 [pii].
57. Lin, L., Chen, K., Abdel Khalek, W., Ward, J.L., 3rd, Yang, H., Chabi, B., Wrutniak-Cabello, C., and Tong, Q. (2014). Regulation of skeletal muscle oxidative capacity and muscle mass by SIRT3. PLoS One *9*, e85636. 10.1371/journal.pone.0085636.
58. DeFronzo, R.A., and Tripathy, D. (2009). Skeletal muscle insulin resistance is the primary defect in type 2 diabetes. Diabetes Care *32 Suppl 2*, S157-163. 10.2337/dc09-S302.
59. Choi, S.E., Jang, H.J., Kang, Y., Jung, J.G., Han, S.J., Kim, H.J., Kim, D.J., and Lee, K.W. (2010). Atherosclerosis induced by a high-fat diet is alleviated by lithium chloride via reduction of VCAM expression in ApoE-deficient mice. Vascul Pharmacol *53*, 264-272. 10.1016/j.vph.2010.09.004.
60. Henriksen, E.J., and Dokken, B.B. (2006). Role of glycogen synthase kinase-3 in insulin resistance and type 2 diabetes. Curr Drug Targets *7*, 1435-1441. 10.2174/1389450110607011435.
61. Pearce, N.J., Arch, J.R., Clapham, J.C., Coghlan, M.P., Corcoran, S.L., Lister, C.A., Llano, A., Moore, G.B., Murphy, G.J., Smith, S.A., et al. (2004). Development of glucose intolerance in male transgenic mice overexpressing human glycogen synthase kinase-3beta on a muscle-specific promoter. Metabolism *53*, 1322-1330. 10.1016/j.metabol.2004.05.008.
62. Duan, X., Norris, D.M., Humphrey, S.J., Yang, P., Cooke, K.C., Bultitude, W.P., Parker, B.L., Conway, O.J., Burchfield, J.G., Krycer, J.R., et al. (2022). Trafficking regulator of GLUT4-1 (TRARG1) is a GSK3 substrate. Biochem J *479*, 1237-1256. 10.1042/bcj20220153.
63. Lee, J., and Kim, M.S. (2007). The role of GSK3 in glucose homeostasis and the development of insulin resistance. Diabetes Res Clin Pract *77 Suppl 1*, S49-57. 10.1016/j.diabres.2007.01.033.
64. Matthews, E., Brassington, R., Kuntzer, T., Jichi, F., and Manzur, A.Y. (2016). Corticosteroids for the treatment of Duchenne muscular dystrophy. Cochrane Database Syst Rev *2016*, Cd003725. 10.1002/14651858.CD003725.pub4.
65. Birnkrant, D.J., Bushby, K., Bann, C.M., Apkon, S.D., Blackwell, A., Brumbaugh, D., Case, L.E., Clemens, P.R., Hadjiyannakis, S., Pandya, S., et al. (2018). Diagnosis and management of Duchenne muscular dystrophy, part 1: diagnosis, and neuromuscular, rehabilitation, endocrine, and gastrointestinal and nutritional management. Lancet Neurol *17*, 251-267. 10.1016/s1474-4422(18)30024-3.
66. Weber, D.R., Hadjiyannakis, S., McMillan, H.J., Noritz, G., and Ward, L.M. (2018). Obesity and Endocrine Management of the Patient With Duchenne Muscular Dystrophy. Pediatrics *142*, S43-s52. 10.1542/peds.2018-0333F.

67. Zhang, T., and Kong, X. (2021). Recent advances of glucocorticoids in the treatment of Duchenne muscular dystrophy (Review). Exp Ther Med *21*, 447. 10.3892/etm.2021.9875.
68. Rana, A.K., and Singh, D. (2018). Targeting glycogen synthase kinase-3 for oxidative stress and neuroinflammation: Opportunities, challenges and future directions for cerebral stroke management. Neuropharmacology *139*, 124-136. 10.1016/j.neuropharm.2018.07.006.
69. Potz, B.A., Scrimgeour, L.A., Sabe, S.A., Clements, R.T., Sodha, N.R., and Sellke, F.W. (2018). Glycogen synthase kinase 3β inhibition reduces mitochondrial oxidative stress in chronic myocardial ischemia. J Thorac Cardiovasc Surg *155*, 2492-2503. 10.1016/j.jtcvs.2017.12.127.
70. Zhazykbayeva, S., Pabel, S., Mügge, A., Sossalla, S., and Hamdani, N. (2020). The molecular mechanisms associated with the physiological responses to inflammation and oxidative stress in cardiovascular diseases. Biophys Rev *12*, 947-968. 10.1007/s12551-020-00742-0.
71. Bagdatlioglu, E., Porcari, P., Greally, E., Blamire, A.M., and Straub, V.W. (2020). Cognitive impairment appears progressive in the mdx mouse. Neuromuscul Disord *30*, 368-388. 10.1016/j.nmd.2020.02.018.
72. Comim, C.M., Ventura, L., Freiberger, V., Dias, P., Bragagnolo, D., Dutra, M.L., Amaral, R.A., Camargo-Fagundes, A.L.S., Reis, P.A., Castro-Faria-Neto, H.C., et al. (2019). Neurocognitive Impairment in mdx Mice. Mol Neurobiol. 10.1007/s12035-019-1573-7.
73. Remmelink, E., Aartsma-Rus, A., Smit, A.B., Verhage, M., Loos, M., and van Putten, M. (2016). Cognitive flexibility deficits in a mouse model for the absence of full-length dystrophin. Genes Brain Behav *15*, 558-567. 10.1111/gbb.12301.
74. Wilson, E.N., Do Carmo, S., Iulita, M.F., Hall, H., Ducatenzeiler, A., Marks, A.R., Allard, S., Jia, D.T., Windheim, J., and Cuello, A.C. (2017). BACE1 inhibition by microdose lithium formulation NP03 rescues memory loss and early stage amyloid neuropathology. Transl Psychiatry *7*, e1190. 10.1038/tp.2017.169.
75. Yu, F., Zhang, Y., and Chuang, D.M. (2012). Lithium reduces BACE1 overexpression, β amyloid accumulation, and spatial learning deficits in mice with traumatic brain injury. J Neurotrauma *29*, 2342-2351. 10.1089/neu.2012.2449.
76. Chatterjee, S., and Mudher, A. (2018). Alzheimer's Disease and Type 2 Diabetes: A Critical Assessment of the Shared Pathological Traits. Front Neurosci *12*, 383. 10.3389/fnins.2018.00383.
77. Pugazhenthi, S., Qin, L., and Reddy, P.H. (2017). Common neurodegenerative pathways in obesity, diabetes, and Alzheimer's disease. Biochim Biophys Acta Mol Basis Dis *1863*, 1037-1045. 10.1016/j.bbadis.2016.04.017.
78. Yoon, S.S., and Jo, S.A. (2012). Mechanisms of Amyloid-β Peptide Clearance: Potential Therapeutic Targets for Alzheimer's Disease. Biomol Ther (Seoul) *20*, 245-255. 10.4062/biomolther.2012.20.3.245.
79. Horrigan, J., Gomes, T.B., Snape, M., Nikolenko, N., McMorn, A., Evans, S., Yaroshinsky, A., Della Pasqua, O., Oosterholt, S., and Lochmüller, H. (2020). A Phase 2 Study of AMO-02 (Tideglusib) in Congenital and Childhood-Onset Myotonic Dystrophy Type 1 (DM1). Pediatr Neurol *112*, 84-93. 10.1016/j.pediatrneurol.2020.08.001.

80. Baranowski, R.W., Braun, J.L., Vandenboom, R., and Fajardo, V.A. (2022). Neurogranin inhibits calcineurin in murine soleus muscle: Effects of heterozygous knockdown on muscle adaptations to tenotomy and fatigue resistance. Biochemical and Biophysical Research Communications *623*, 89-95. https://doi.org/10.1016/j.bbrc.2022.07.062.
81. Bigard, X., Sanchez, H., Zoll, J., Mateo, P., Rousseau, V., Veksler, V., and Ventura-Clapier, R. (2000). Calcineurin Co-regulates contractile and metabolic components of slow muscle phenotype. J Biol Chem *275*, 19653-19660. 10.1074/jbc.M000430200.
82. Long, Y.C., Glund, S., Garcia-Roves, P.M., and Zierath, J.R. (2007). Calcineurin regulates skeletal muscle metabolism via coordinated changes in gene expression. J Biol Chem *282*, 1607-1614. 10.1074/jbc.M609208200.
83. Talmadge, R.J., Otis, J.S., Rittler, M.R., Garcia, N.D., Spencer, S.R., Lees, S.J., and Naya, F.J. (2004). Calcineurin activation influences muscle phenotype in a muscle-specific fashion. BMC Cell Biol *5*, 28. 10.1186/1471-2121-5-28

1471-2121-5-28 [pii].
84. Fajardo, V.A., Gamu, D., Rietze, B.A., Kwon, F., Chamebrs, P.J., Quadrilatero, J., Tupling, A.R. (2016). Sarcolipin Deletion in mdx mice Worsens Dystrophic Pathology by Impairing Calcineurin Signaling and Reducing Utrophin Expression. FASEB J *30*, 1224.1226.
85. Stupka, N., Schertzer, J.D., Bassel-Duby, R., Olson, E.N., and Lynch, G.S. (2008). Stimulation of calcineurin Aalpha activity attenuates muscle pathophysiology in mdx dystrophic mice. Am J Physiol Regul Integr Comp Physiol *294*, R983-992. 10.1152/ajpregu.00375.2007.
86. Rommel, C., Bodine, S.C., Clarke, B.A., Rossman, R., Nunez, L., Stitt, T.N., Yancopoulos, G.D., and Glass, D.J. (2001). Mediation of IGF-1-induced skeletal myotube hypertrophy by PI(3)K/Akt/mTOR and PI(3)K/Akt/GSK3 pathways. Nat Cell Biol *3*, 1009-1013. 10.1038/ncb1101-1009.
87. Shen, T., Cseresnyes, Z., Liu, Y., Randall, W.R., and Schneider, M.F. (2007). Regulation of the nuclear export of the transcription factor NFATc1 by protein kinases after slow fibre type electrical stimulation of adult mouse skeletal muscle fibres. J Physiol *579*, 535-551. 10.1113/jphysiol.2006.120048.
88. Hammer, S., Toussaint, M., Vollsæter, M., Nesbjørg Tvedt, M., Drange Røksund, O., Reychler, G., Lund, H., and Andersen, T. (2022). Exercise Training in Duchenne Muscular Dystrophy: A Systematic Review and Meta-Analysis. J Rehabil Med *54*, jrm00250. 10.2340/jrm.v53.985.
89. Lei, P., Ayton, S., Bush, A.I., and Adlard, P.A. (2011). GSK-3 in Neurodegenerative Diseases. Int J Alzheimers Dis *2011*, 189246. 10.4061/2011/189246.
90. Geromella, M.S., Ryan, C.R., Braun, J.L., Finch, M.S., Maddalena, L.A., Bagshaw, O., Hockey, B.L., Moradi, F., Fenech, R.K., Ryoo, J., et al. (2022). Low-dose lithium supplementation promotes adipose tissue browning and sarco(endo)plasmic reticulum Ca(2+) ATPase uncoupling in muscle. J Biol Chem *298*, 102568. 10.1016/j.jbc.2022.102568.
91. Mathis, A., Mamidanna, P., Cury, K.M., Abe, T., Murthy, V.N., Mathis, M.W., and Bethge, M. (2018). DeepLabCut: markerless pose estimation of user-defined body parts with deep learning. Nat Neurosci *21*, 1281-1289. 10.1038/s41593-018-0209-y.
92. Mendez J, K., A (1960). Density and composition of mammalian muscle. Metabolism *9*, 184-188.

93. Brooks, S.V., and Faulkner, J.A. (1988). Contractile properties of skeletal muscles from young, adult and aged mice. J Physiol *404*, 71-82.
94. Bloemberg, D., and Quadrilatero, J. (2012). Rapid determination of myosin heavy chain expression in rat, mouse, and human skeletal muscle using multicolor immunofluorescence analysis. PLoS One *7*, e35273. 10.1371/journal.pone.0035273

PONE-D-11-20138 [pii].
95. Braun, J.L., Teng, A.C.T., Geromella, M.S., Ryan, C.R., Fenech, R.K., MacPherson, R.E.K., Gramolini, A.O., and Fajardo, V.A. (2021). Neuronatin promotes SERCA uncoupling and its expression is altered in skeletal muscles of high-fat diet-fed mice. FEBS Lett *595*, 2756-2767. 10.1002/1873-3468.14213.
96. Geromella, M.S., Braun, J.L., and Fajardo, V.A. (2023). Measuring SERCA-mediated calcium uptake in mouse muscle homogenates. STAR Protoc *4*, 101987. 10.1016/j.xpro.2022.101987.
97. Acin-Perez, R., Benador, I.Y., Petcherski, A., Veliova, M., Benavides, G.A., Lagarrigue, S., Caudal, A., Vergnes, L., Murphy, A.N., Karamanlidis, G., et al. (2020). A novel approach to measure mitochondrial respiration in frozen biological samples. EMBO J *39*, e104073. 10.15252/embj.2019104073.
98. Osto, C., Benador, I.Y., Ngo, J., Liesa, M., Stiles, L., Acin-Perez, R., and Shirihai, O.S. (2020). Measuring Mitochondrial Respiration in Previously Frozen Biological Samples. Curr Protoc Cell Biol *89*, e116. 10.1002/cpcb.116.
99. Fajardo, V.A., Bombardier, E., McMillan, E., Tran, K., Wadsworth, B.J., Gamu, D., Hopf, A., Vigna, C., Smith, I.C., Bellissimo, C., et al. (2015). Phospholamban overexpression in mice causes a centronuclear myopathy-like phenotype. Dis Model Mech *8*, 999-1009. 10.1242/dmm.020859.

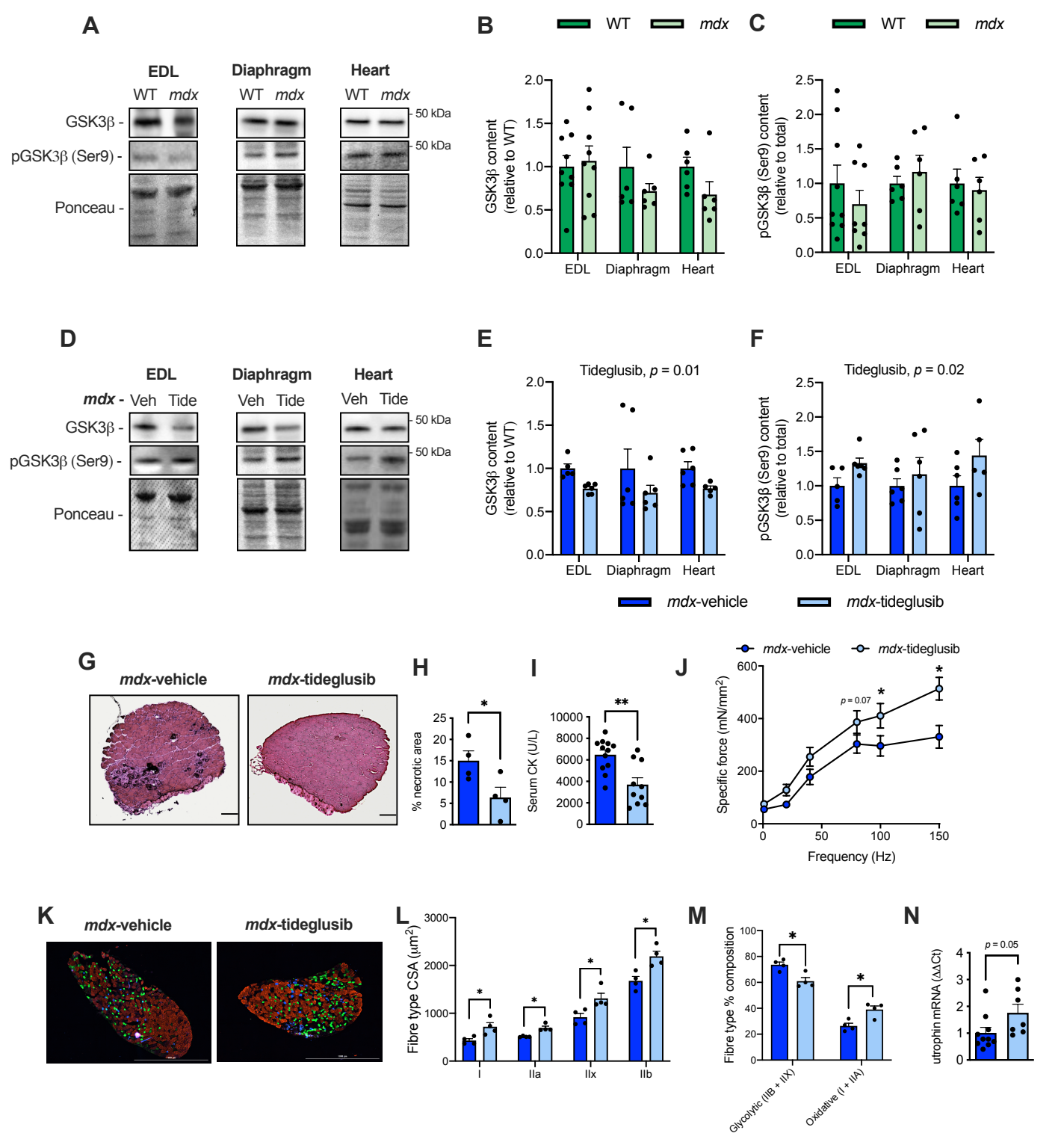
A
EDL
Diaphragm
Heart
WT mdx
GSK3β -
pGSK3β (Ser9) -
Ponceau -
50 kDa
B
WT
mdx
GSK3β content (relative to WT)
EDL
Diaphragm
Heart
C
pGSK3β (Ser9) content (relative to total)
D
mdx - Veh Tide
E
Tideglusib, p = 0.01
F
Tideglusib, p = 0.02
mdx-vehicle
mdx-tideglusib
G
H
% necrotic area
I
Serum CK (U/L)
J
Specific force (mN/mm2)
Frequency (Hz)
p = 0.07
K
L
Fibre type CSA (μm2)
I
IIa
IIx
IIb
M
Fibre type % composition
Glycolytic (IIB + IIX)
Oxidative (I + IIA)
N
utrophin mRNA (ΔΔCt)
p = 0.05

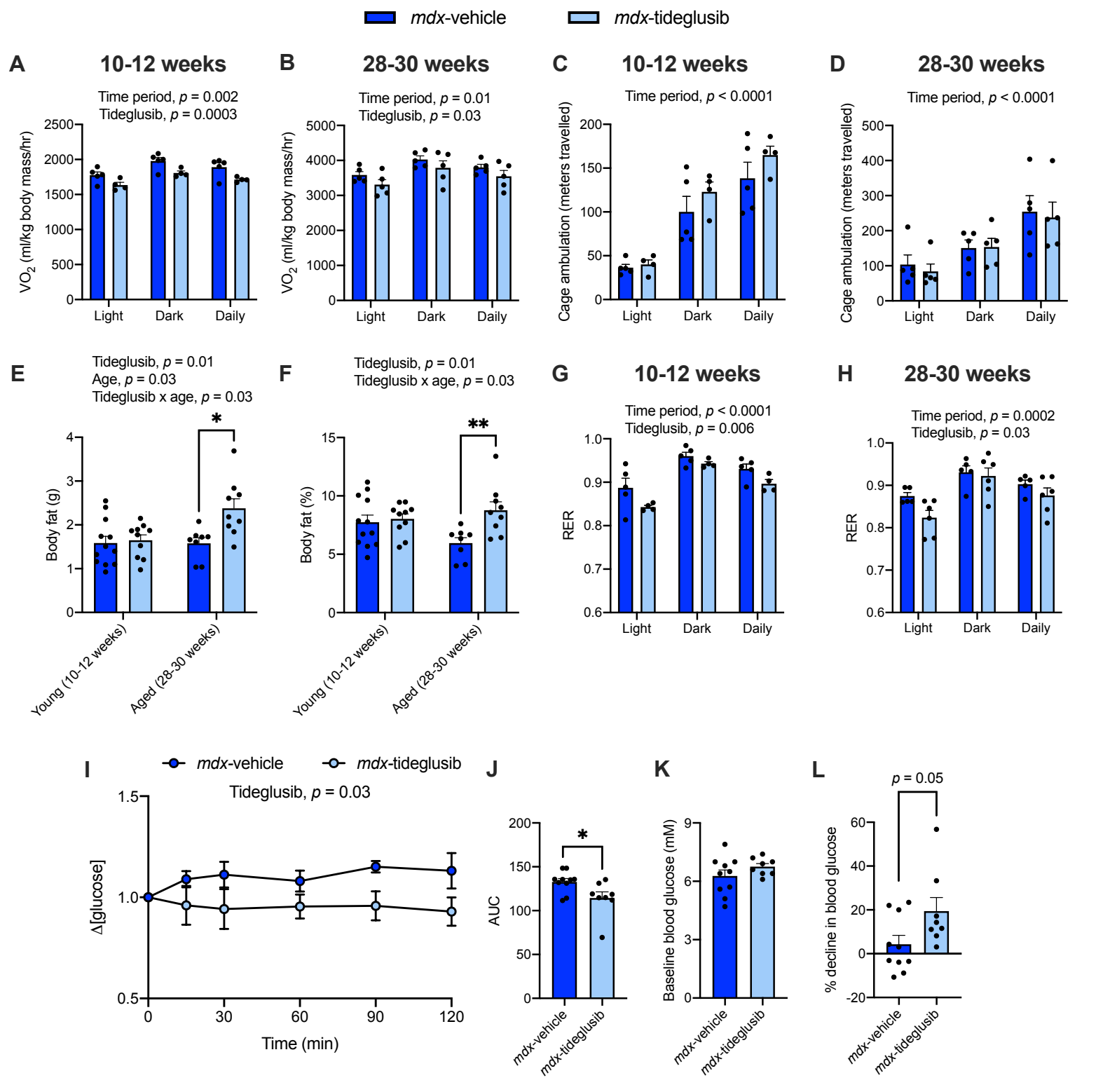
mdx-vehicle
mdx-tideglusib
A
10-12 weeks
Time period, p = 0.002
Tideglusib, p = 0.0003
VO2 (ml/kg body mass/hr)
Light
Dark
Daily
B
28-30 weeks
Time period, p = 0.01
Tideglusib, p = 0.03
C
10-12 weeks
Time period, p < 0.0001
Cage ambulation (meters travelled)
D
28-30 weeks
Time period, p < 0.0001
E
Tideglusib, p = 0.01
Age, p = 0.03
Tideglusib x age, p = 0.03
Body fat (g)
Young (10-12 weeks)
Aged (28-30 weeks)
F
Tideglusib, p = 0.01
Tideglusib x age, p = 0.03
Body fat (%)
G
10-12 weeks
Time period, p < 0.0001
Tideglusib, p = 0.006
RER
H
28-30 weeks
Time period, p = 0.0002
Tideglusib, p = 0.03
I
Tideglusib, p = 0.03
Δ[glucose]
Time (min)
J
AUC
K
Baseline blood glucose (mM)
L
p = 0.05
% decline in blood glucose

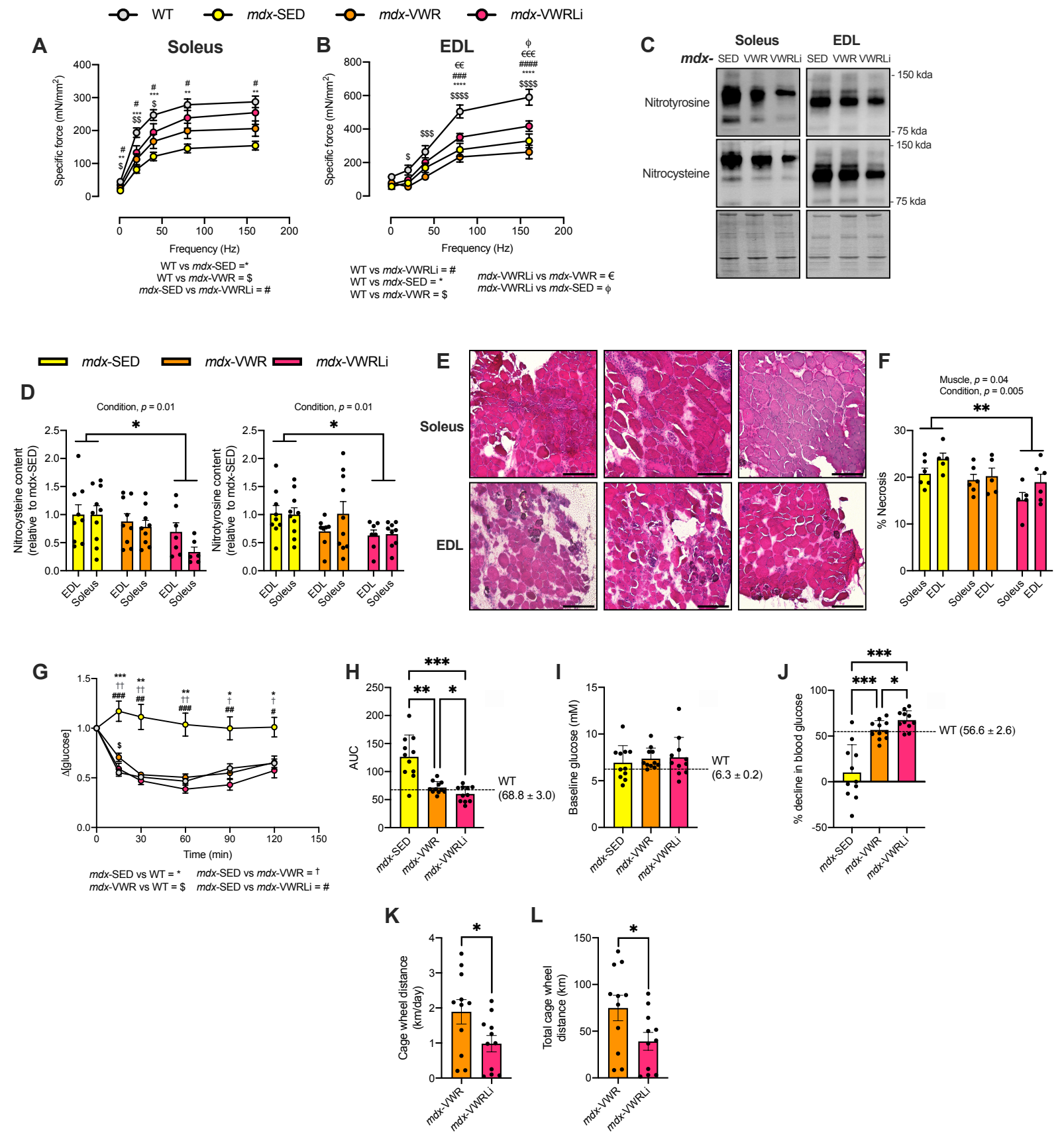
WT
mdx-SED
mdx-VWR
mdx-VWRLi
A
Soleus
Specific force (mN/mm²)
Frequency (Hz)
WT vs mdx-SED =*
WT vs mdx-VWR = $
mdx-SED vs mdx-VWRLi = #
B
EDL
Specific force (mN/mm²)
Frequency (Hz)
WT vs mdx-VWRLi = #
WT vs mdx-SED = *
WT vs mdx-VWR = $
mdx-VWRLi vs mdx-VWR = €
mdx-VWRLi vs mdx-SED = ϕ
C
Soleus
EDL
mdx- SED VWR VWRLi SED VWR VWRLi
Nitrotyrosine
Nitrocysteine
150 kda
75 kda
150 kda
75 kda
mdx-SED
mdx-VWR
mdx-VWRLi
D
Condition, p = 0.01
Nitrocysteine content (relative to mdx-SED)
Condition, p = 0.01
Nitrotyrosine content (relative to mdx-SED)
EDL
Soleus
E
Soleus
EDL
F
Muscle, p = 0.04
Condition, p = 0.005
% Necrosis
Soleus
EDL
G
Δ[glucose]
Time (min)
mdx-SED vs WT = *
mdx-SED vs mdx-VWR = †
mdx-VWR vs WT = $
mdx-SED vs mdx-VWRLi = #
H
AUC
WT (68.8 ± 3.0)
mdx-SED
mdx-VWR
mdx-VWRLi
I
Baseline glucose (mM)
WT (6.3 ± 0.2)
mdx-SED
mdx-VWR
mdx-VWRLi
J
% decline in blood glucose
WT (56.6 ± 2.6)
mdx-SED
mdx-VWR
mdx-VWRLi
K
Cage wheel distance (km/day)
mdx-VWR
mdx-VWRLi
L
Total cage wheel distance (km)
mdx-VWR
mdx-VWRLi

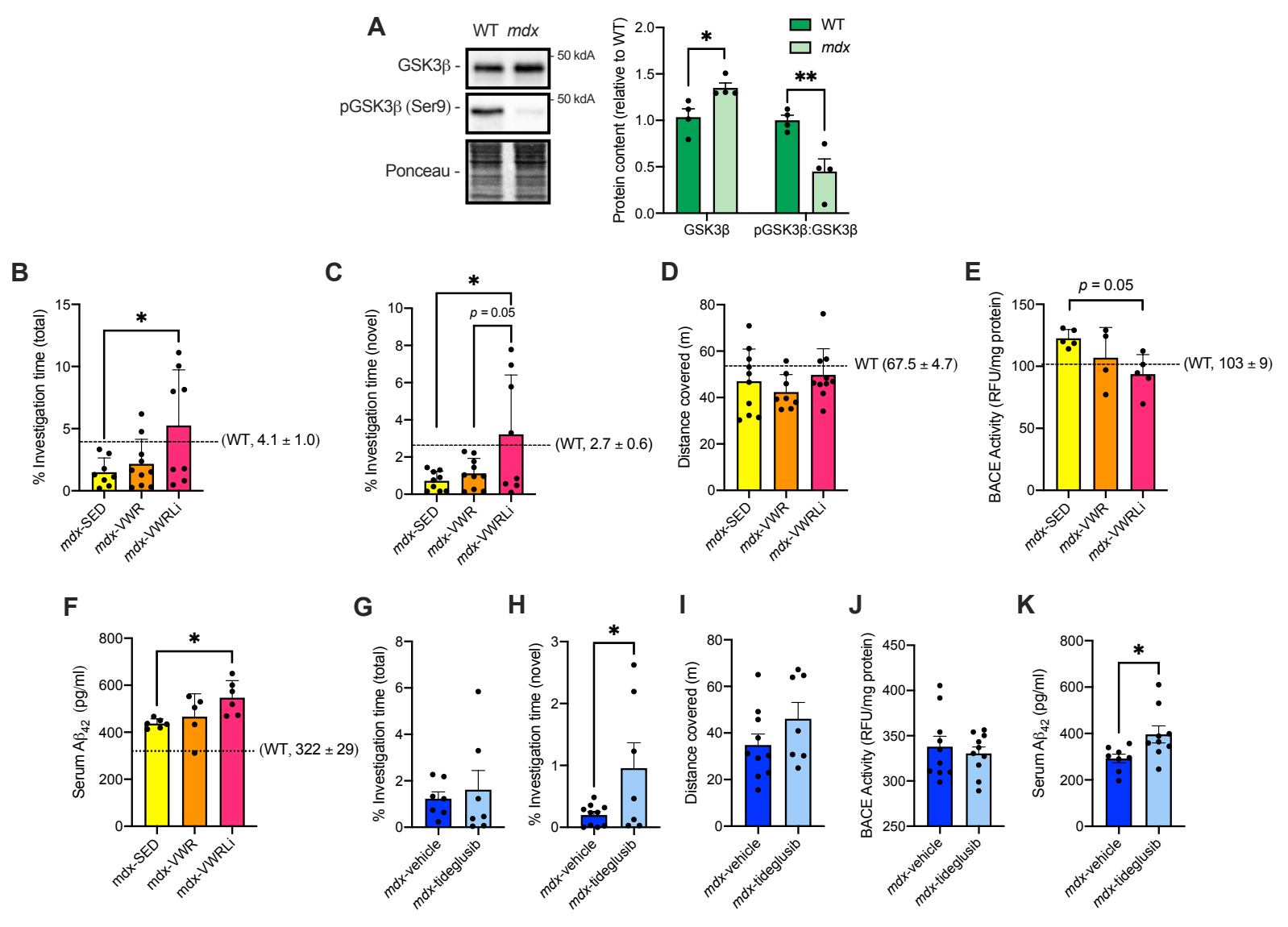
A
WT mdx
GSK3β -
pGSK3β (Ser9) -
Ponceau -
50 kDA
50 kDA
Protein content (relative to WT)
WT
mdx
GSK3β
pGSK3β:GSK3β
B
% Investigation time (total)
(WT, 4.1 ± 1.0)
mdx-SED
mdx-VWR
mdx-VWRLi
C
% Investigation time (novel)
p = 0.05
(WT, 2.7 ± 0.6)
D
Distance covered (m)
WT (67.5 ± 4.7)
E
BACE Activity (RFU/mg protein)
p = 0.05
(WT, 103 ± 9)
F
Serum Aβ42 (pg/ml)
(WT, 322 ± 29)
G
% Investigation time (total)
mdx-vehicle
mdx-tideglusib
H
% Investigation time (novel)
I
Distance covered (m)
J
BACE Activity (RFU/mg protein)
K
Serum Aβ42 (pg/ml)